AD-A097 355 TEXAS UNIV AT AUSTIN DEPT OF ELECTRICAL ENGINEERING F/G 9/3
QUASI-OPTICAL TECHNIQUES FOR MILLIMETER AND SUBMILLIMETER-WAVE --ETC(U)
MAR 81 T ITOH DAAG29-78-G-0145
UNCLASSIFIED ARO-16171.17-EL NL

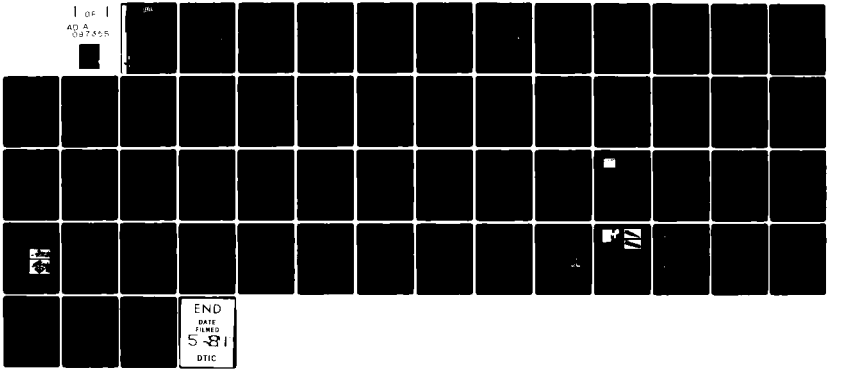

12
B.S.

QUASI-OPTICAL TECHNIQUES FOR MILLIMETER AND SUBMILLIMETER-WAVE CIRCUITS

FINAL REPORT

by

TATSUO ITOH

MARCH 25, 1981

US ARMY RESEARCH OFFICE

GRANT NO. DAAG29-78-G-0145

UNIVERSITY OF TEXAS
DEPT. OF ELECTRICAL ENGINEERING
P.O. BOX 7728
AUSTIN, TEXAS 78712

12

QUASI-OPTICAL TECHNIQUES FOR MILLIMETER AND SUBMILLIMETER-WAVE CIRCUITS

FINAL REPORT

by

TATSUO ITOH

MARCH 25, 1981

US ARMY RESEARCH OFFICE

GRANT NO. DAAG29-78-G-0145

UNIVERSITY OF TEXAS
DEPT. OF ELECTRICAL ENGINEERING
P.O. BOX 7728
AUSTIN, TEXAS 78712

SECURITY CLASSIFICATION OF THIS PAGE (When Data Entered)

REPORT DOCUMENTATION PAGE

READ INSTRUCTIONS BEFORE COMPLETING FORM

1. REPORT NUMBER: 16171.17-EL	2. GOVT ACCESSION NO.: AD A097355
3. RECIPIENT'S CATALOG NUMBER:	
4. TITLE (and Subtitle): Quasi-Optical Techniques for Millimeter and Submillimeter-Wave Circuits.	5. TYPE OF REPORT & PERIOD COVERED: Final Report. July 1978-January 1981
	6. PERFORMING ORG. REPORT NUMBER:
7. AUTHOR(s): Tatsuo Itoh	8. CONTRACT OR GRANT NUMBER(s): DAAG29-78-G-0145
9. PERFORMING ORGANIZATION NAME AND ADDRESS: University of Texas, P.O. Box 7728, Austin, Texas 78712	10. PROGRAM ELEMENT, PROJECT, TASK AREA & WORK UNIT NUMBERS
11. CONTROLLING OFFICE NAME AND ADDRESS: U.S. Army Research Office, Post Office Box 12211, Research Triangle Park, NC 27709	12. REPORT DATE: March 25, 1981 13. NUMBER OF PAGES:
14. MONITORING AGENCY NAME & ADDRESS (if different from Controlling Office)	15. SECURITY CLASS. (of this report): Unclassified 15a. DECLASSIFICATION/DOWNGRADING SCHEDULE: N/A

16. DISTRIBUTION STATEMENT (of this Report)

Approved for public release; distribution unlimited.

17. DISTRIBUTION STATEMENT (of the abstract entered in Block 20, if different from Report)

NA

18. SUPPLEMENTARY NOTES

The findings in this report are not to be construed as an official Department of the Army position, unless so designated by other authorized documents.

19. KEY WORDS (Continue on reverse side if necessary and identify by block number)

Distributed Bragg reflector, Gunn diode, Dielectric waveguide, Image guide, Trapped image guide, Inverted strip dielectric guide, Leaky-wave antenna, Yagi-Uda array, Half-wave slot, Printed lines, Patch antennas

20. ABSTRACT (Continue on reverse side if necessary and identify by block number)

This report summarizes research activities at the Microwave Laboratory, University of Texas on various structures for millimeter-wave and submillimeter-wave circuits under sponsorship of US Army Research Office Grant DAAG29-78-G-0145. The topics of investigation include distributed feedback oscillators, distributed gain mechanisms, trapped image guides and leaky wave antennas, monolithic detectors, excitation of dielectric waveguides, printed lines and printed radiating structures. A list of publications is included.

DD FORM 1 JAN 73 1473 EDITION OF 1 NOV 65 IS OBSOLETE

Unclassified

SECURITY CLASSIFICATION OF THIS PAGE (When Data Entered)

401 997

TABLE OF CONTENTS

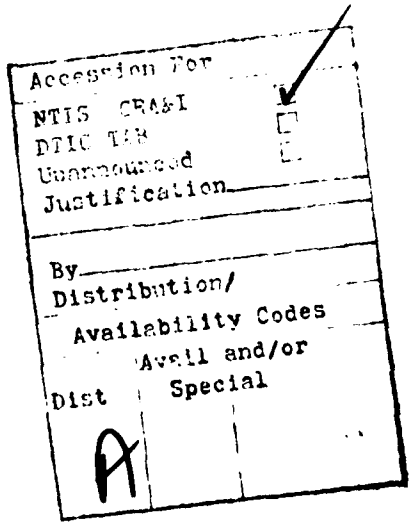

LIST OF FIGURES

LIST OF APPENDICES

Abstract

This report summarizes research activities at the Microwave Laboratory, University of Texas on various structures for millimeter-wave and submillimeter-wave circuits under sponsorship of US Army Research Office Grant DAAG29-78-G-0145. The topics of investigation include distributed feedback oscillators, distributed gain mechanisms, trapped image guides and leaky wave antennas, monolithic detectors, excitation of dielectric waveguides, printed lines and printed radiating structures. A list of publications is included.

1. Introduction

In the past several years, a considerable attention has been paid on the millimeter-wave devices, components and systems. It is preferable to use integrated circuit approaches for a number of reasons. The integrated circuit approaches may be classified into two broad categories. One of them is based on the printed transmission lines and another on dielectric waveguides. The former is an extension of the microwave integrated circuits. As the frequency of operation is increased, the structures based on this approach become smaller and smaller and the loss associated with metal conductors will increase. The cost of fabrication of these structures will increase sharply with the frequency. Presently, many impressive results have been obtained for the frequency range up to 300 GHz especially in the area of low noise mixers.[1]

On the other hand, the dielectric waveguide techniques are millimeter-wave replica of optical integrated circuits. Components made by this technique can be much larger than the printed line counterparts. Since this technique is based on optical principle, the performances of the structures are more effective as the frequency of operation is increased. The single most important problem in this technique is the radiation loss which arises at any discontinuities and bends. This problem is especially taxing when an active device is being implemented. Because most active devices are made for waveguide or printed line and are usually small as compared to the wavelength, an abrupt junction is created in the dielectric waveguide. Another important problem is the interfacing of dielectric waveguides with printed lines. Needs for such interfacing occur when RF and IF frequency signals are to be handled and when a bias line is to be implemented for a solid state device.

In this report, we describe several topics, studied under the sponsorship of the Grant DAAG29-78-G-0145, which address themselves to better utilization of millimeter-wave spectrum by providing analysis and design of existing as well as new structures.

2. Dielectric Waveguide Structures

In this chapter, we describe several innovative structures which provide alternatives to existing millimeter-wave components. The basis of these structures is an analysis of the dielectric waveguide structure. We will summarize here this analysis to lay the foundation for discussion of dielectric waveguide components. Since the details of the analysis are given in literature,[2,3] only the key step is presented here. Fig. 1 is the cross section of a trapped image guide. (The detail of this waveguide will be given later in this chapter.) When $c \to \infty$, we recover a conventional image guide. It is known that E^y and E^x modes can propagate in this structure. For the former the principal electric field is in the y direction. We will apply the method of effective dielectric constant for the image guide ($c \to \infty$).

The complete field components in this waveguide may be derived from two field components:

$$E_y = \frac{1}{\varepsilon_i} \left(\beta^2 - \frac{\partial^2}{\partial x^2}\right)\phi^e \tag{1}$$

$$H_y = \left(\beta^2 - \frac{\partial^2}{\partial x^2}\right)\phi^h \tag{2}$$

where ε_i is the relative dielectric constant in each constituent region in Fig. 1, β is the propagation constant and ϕ^e and ϕ^h are two scalar potentials. For E^y mode, where E_y and H_x are predominant, we neglect H_y by letting $\phi^h = 0$. Next, we obtain the effective dielectric constant (EDC) of regions 1 and 2.

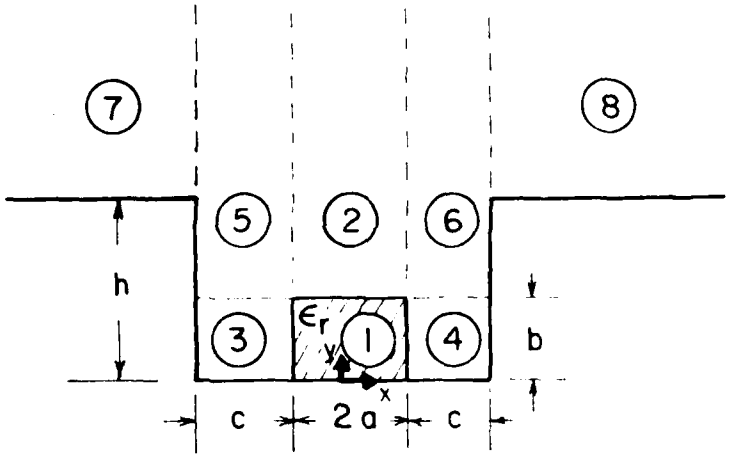

Figure 1. Cross section of a trapped image guide

To this end, we assume that [illegible] write field expressions for the slab waveguide [illegible] verb makes it possible to derive [illegible]

(2)

where k_y is the [illegible] structure. Once, the [illegible] regions 1 and 2 with a vertical slit of [illegible] β_{ep}. Now, we solve the [illegible] solution to which gives the propagation [illegible]. Although the answers are [illegible] of the most practical applications [illegible] the image guide obtained by this method.

With this background [illegible] we studied during this [illegible]

2.1 Distributed Bragg [illegible]

It has been proposed [illegible] the dielectric waveguide and [illegible] guide, a stepband is created. [illegible] propagation constant and d is the period [illegible] the grating section from [illegible] reflection occurs only [illegible] wavelengths, the grating [illegible] distributed Bragg reflector [illegible]. In this structure, a [illegible] from the ground plane [illegible] computed and

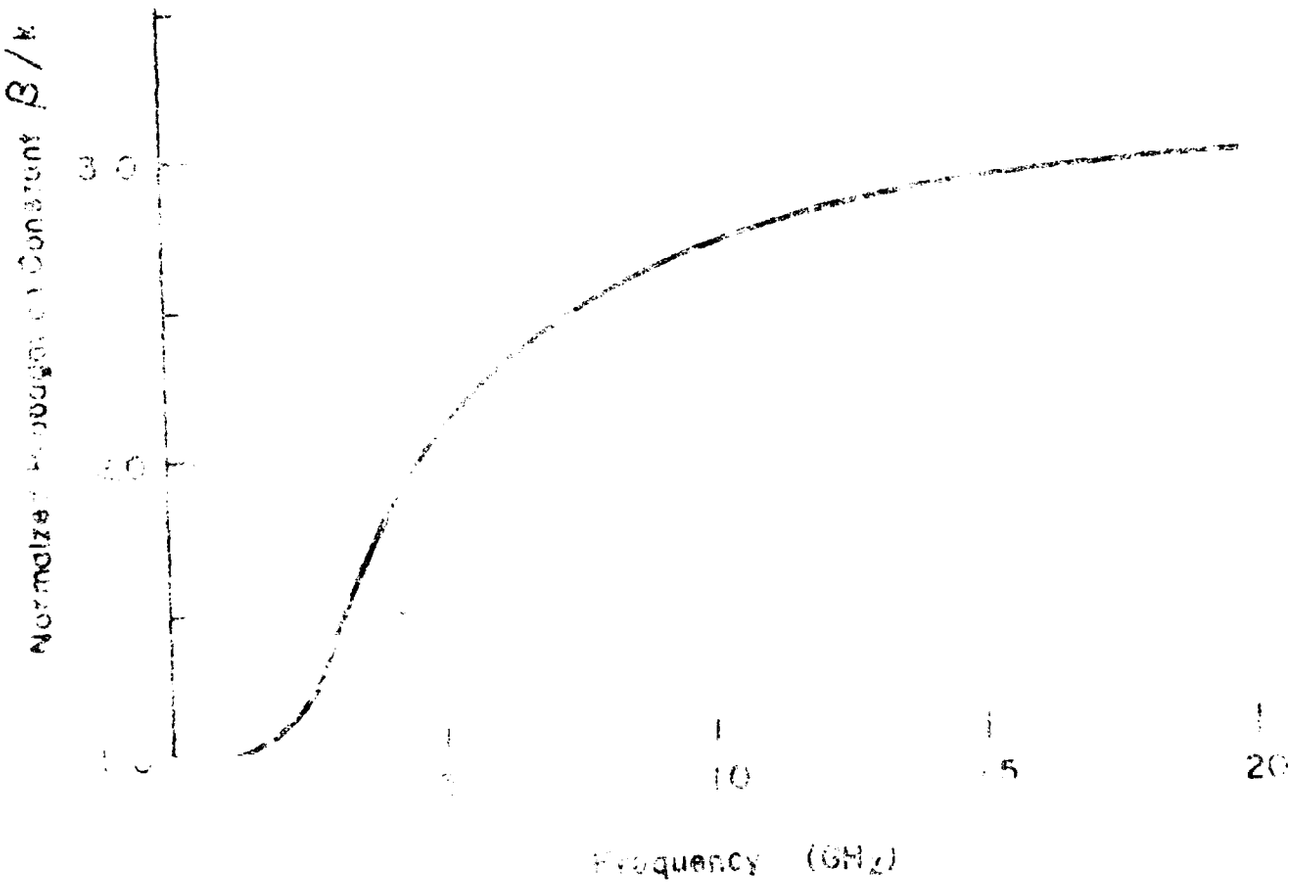

Figure 2. Typical dispersion characteristic for an image guide

the length [illegible] determined [illegible] on both [illegible] grating structure [illegible] only when the [illegible] at such [illegible] Hence, the [illegible] able than that [illegible] oscillation condition is [illegible]

$$[illegible] \quad (4)$$

$$[illegible] \quad (5)$$

where [illegible] are the [illegible] of the diode and [illegible] are the total [illegible] diode. The procedure [illegible] Appendix [illegible]

The distributed [illegible] may [illegible] way that one of the reflectors [illegible] This is accomplished by [illegible] at 2d. For the [illegible] this modified [illegible] called leaky-wave [illegible] the broadside direction, but [illegible] grating provides a strong feedback to the [illegible] broadside firing antenna.[1]

2.2. Measurement of [illegible]

Since the [illegible] a function [illegible] nature of the waveguide, we can [illegible] waveguide material [illegible] measured.

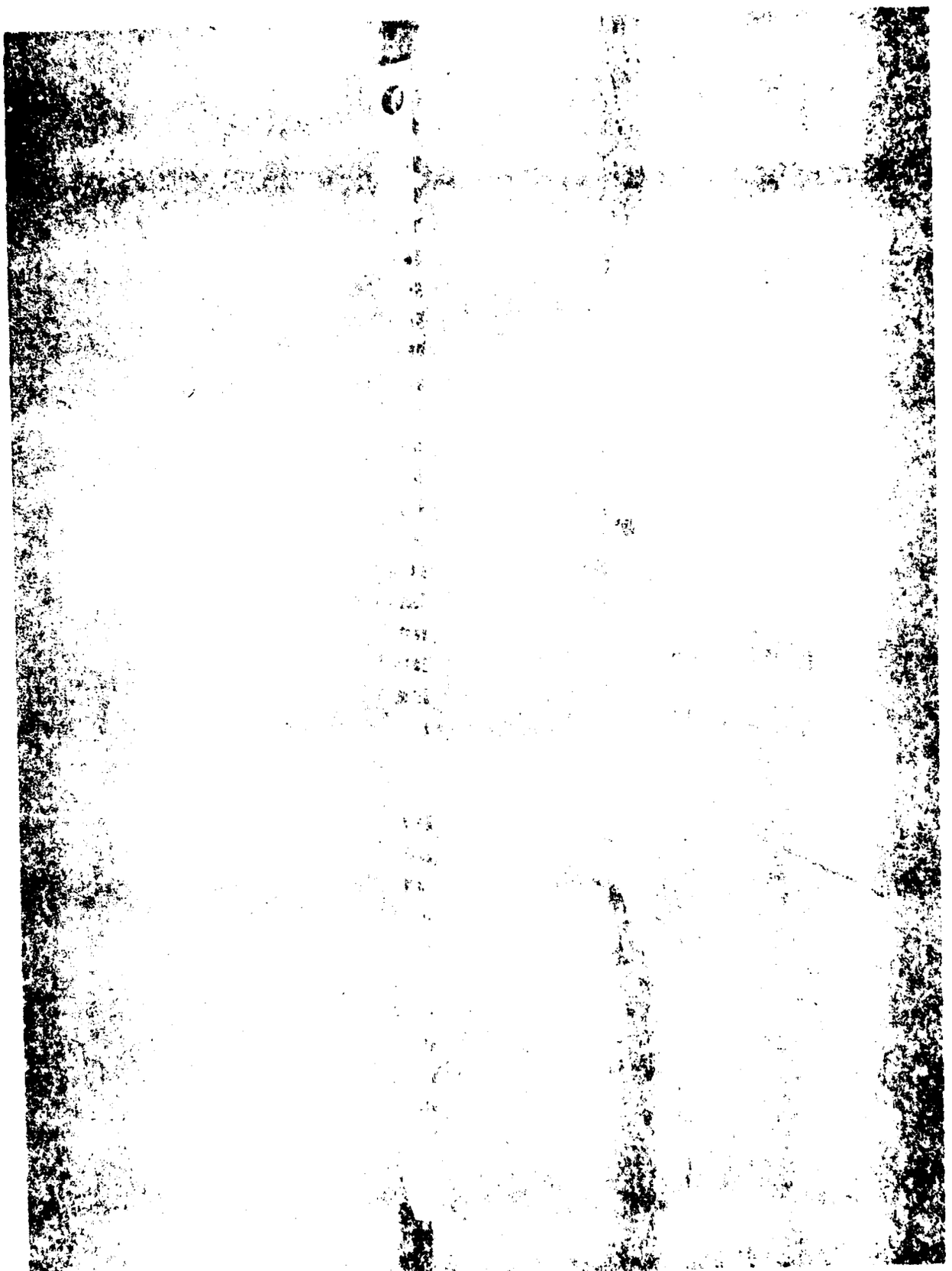

In this project, we used an inverted strip dielectric (IS) waveguide[2] rather than an image guide. This is because the former permits non-destructive measurement. The cross section of the IS guide is shown in Fig. 4. We create a notch-type grating in the dielectric strip (ϵ_1). Then, we place a slab material to be measured with unknown ϵ_2 on top of ϵ_1 to form a guiding layer. This method yielded reasonably accurate answers with a relatively simple setup and an efficient numerical inversion algorithm.[6] The details are given in Appendix 2.

2.3 Resonant frequencies of a dielectric rectangular cavity

The resonant frequency of a dielectric cavity made of a truncated rectangular dielectric waveguide has been analyzed by employing the open circuit (magnetic wall) boundary conditions at the end surfaces. In this project, we obtained improved data on the resonant frequency by imposing a more realistic impedance boundary condition. In addition, we obtained the field variation along the axial direction of the cavity. The results are believed useful for millimeter-wave integrated circuit design.[7]

2.4 Trapped image guide

In this project, a new dielectric waveguide has been developed in which the radiation loss at bends is much smaller than in the conventional image guides.[3] The cross section of the new waveguide is shown in Fig. 1. The structure consists of a dielectric rod placed in a metal trough.

In integrated circuit applications, the image guide must be bent in the transverse direction so as to accomplish designated functions. The image guide has an inherent radiation loss at bends as the electromagnetic energy escapes from the guide as a propagating wave in the sideward direction. In the trapped image guide, such a leakage is mostly reflected back to the dielectric portion

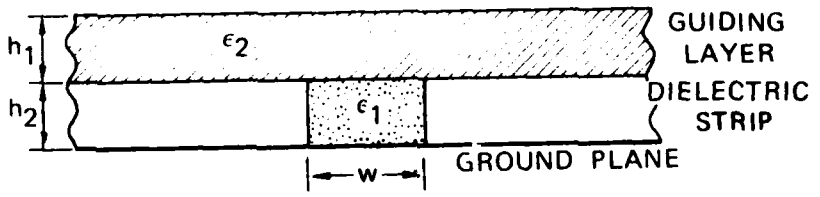

Figure 4. Cross section of an inverted strip dielectric waveguide

by the metal walls if their height h in Fig. 1 is reasonably large. As long as the waveguide is operated in the single mode regions, the reflected energy couples to the guide once again.

We first analyzed the propagation characteristics of the trapped image guide by employing the effective dielectric constant method described earlier. Next, the theoretical results have been compared with the experimental data in the Ka band region. It was found that the guide may be designed in such a way that the propagation characteristics are essentially identical to those of the image guide over most of the single mode region. However, the measurement of the radiation loss at a 90° bend indicated reduction of more than 8 dB from that in an image guide setup.

A leaky-wave antenna was also created by using the trapped image guide. The grating was created with narrow metal strips placed on the top surface of the dielectric rod. The main beam direction is given by

$$\theta_M = \sin^{-1}\left(\frac{\beta_n}{k}\right) \tag{6}$$

where

$$\beta_n = \beta + \frac{2n\pi}{d} \tag{7}$$

is the propagation constant of the n-th space harmonic. Usually, n is taken to be -1. Since the main beam direction is a function of frequency, the antenna is frequency-scannable. In this project, we obtained the scan of the beam from -55° to -10° by changing the frequency from about 30 GHz to 40 GHz. The details are given in Appendix 3.

2.5 Directive planar excitation of image guide

Usually, the image guide and other dielectric waveguides are excited by a tapered section inserted into a waveguide horn designed for the least amount of insertion loss and reflection. If, however, solid state devices are incorporated

in or near the dielectric waveguide, the entire structure is more correctly termed as an integrated circuit. In this project, we investigated a novel structure of exciting an image guide from a planar printed network in which solid state devices may be installed. The structure consists of a Yagi-Uda slot array created in the ground plane of the image guide. In this way, only one slot needs to be excited and the remaining parasitic slots provide directivity for the surface wave launched in the image guide. The length of the driving slot can be obtained by viewing it as a short-circuited slot line and computing its dispersion characteristics.[8] Design of slot spacing requires the knowledge of the guide wavelength λg of the image guide. This is obtained by the use of the effective dielectric constant method. The optimum spacing was experimentally found to be $\lambda g/4$.

Experimental investigations revealed that the front-to-back ratios of transmitted power into the image guide are as high as 10 dB, and that the ratio and bandwidth tend to increase by introducing a larger number of director slots.[9] Appendix 4 describes some of the data on this project. Since this work is not completed, it will be carried over to a new contract period.

2.6 Gain enhancement of monolithic millimeter-wave antenna-detector

In this project, a surface wave antenna made of a tapered dielectric rod is attached in front of a half-wave dipole slot. A beam lead detector diode is incorporated in a planar printed line which feeds the slot at its center. Several different dielectric materials have been used for the substrate of the planar circuit and the rod antenna. The experiments have been conducted at 60 GHz. The planar circuit was developed by the standard photo-etching process. Design of the dielectric rods was based on single mode propagation of the dielectric waveguide. The overall length of the rod was typically 3 to 5 free space wavelengths

with a tapered section about half the overall length. The rod was attached to the slot by means of a low loss adhesive.

The radiation patterns of the structure were measured both with or without the dielectric rod. It was found that use of rod increases the directivity up to 10 dB. In addition, the direction of the main beam can be controlled into either the metal side or the substrate side by attaching the rod to the desired side of the planar structure. More details of the structure and the experimental results[10] are found in Appendix 5.

3. Printed Structures

Printed transmission lines are still widely used for millimeter-wave integrated circuits. They are especially well suited for implementing solid-state devices. In addition, these lines can coexist with dielectric waveguide. It is therefore important to know characteristics of these printed structures accurately. During this grant period we developed a simple but accurate method (spectral domain immittance approach) for analyzing these structures[11] and applied it for transmission lines like microstrip lines, suspended lines, fin-lines and others[12-15] as well as for printed antennas.

To illustrate the method, we use Fig. 5 which shows the cross section of the suspended microstrip line with tunable septums. (The quasi-static case for this structure was reported in Reference 12.) The first step is to identify that from

$$E_y(x,y)e^{-j\beta z} = \frac{1}{2\pi}\int_{-\infty}^{\infty} \tilde{E}_y(\alpha,y)e^{-j(\alpha x+\beta z)}d\alpha \qquad (8)$$

all the field components are superpositions of inhomogeneous (in y) plane waves propagating in the direction of θ from the z axis where $\theta = \cos^{-1}(\beta/\sqrt{\alpha^2+\beta^2})$. For each θ, waves may be decomposed into TM-to-y and TE-to-y fields, and the

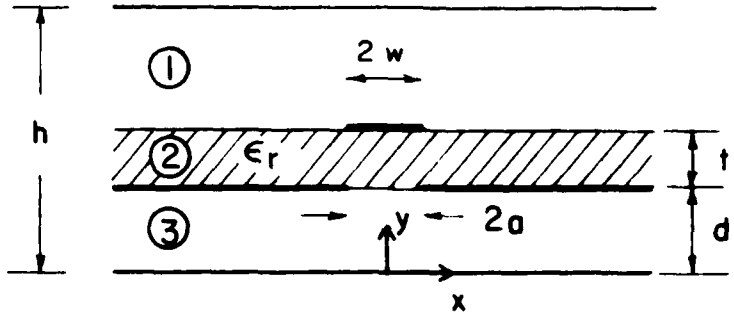

Figure 5. Cross section of a microstrip line with tuning septums

transverse equivalent networks can be shown as in Fig. 6 for both TM and TE components. Relations of the "voltage" and "current" at y=d+t and y=d can be readily obtained by a standard transmission line analysis. Combining these quantitites, we can get the relations between x and z components of current and field at y=d+t and y=d. These relations are nothing out Fourier transforms of tensor Green's functions. We can then apply the Galerkin's method for numerically solving the eigenvalue equation for the structure. The details are given in Appendix 6.

Using this method, we analyzed several printed transmission line structures. For these structures, both the propagation constants and the characteristic impedances have been computed.

Microstrip and coplanar transmission lines made on a GaAs substrate which exhibits negative conductance have been analyzed and compared as to their gain factors, sensitivity, etc. For this study, the quasi-static approximation has been used so that the computation is simple and yet a qualitative information is preserved.[16]

Printed circuit antennas have been of interest for some time. We recognize that, as the operating frequency gets higher, the radiating characteristics become more complicated because of the existence of the surface wave type fields. We adopted the spectral domain immittance approach to printed patch structures. Development of the Green's functions is formally identical to the one discussed earlier. The eigenvalue problem is solved for the complex resonant frequency, the imaginary part of which gives the radiation Q. The far field pattern can be readily obtained from the Fourier transform of the aperture field which in turn can be derived once the eigenvalue equation is solved.[17]

The method was modified to analyze a circular patch radiating structure. The procedure is essentially identical although the Hankel transforms need to

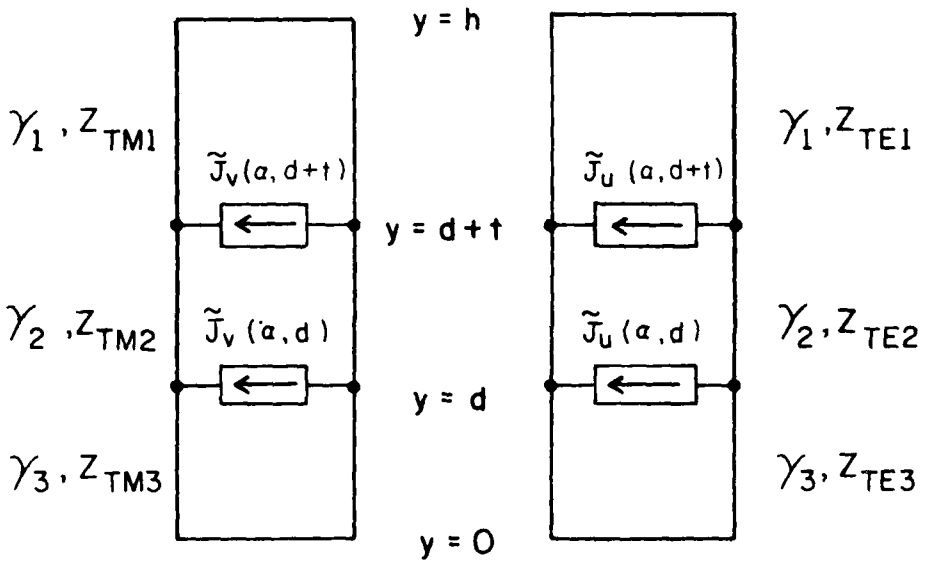

Figure 6. Transverse equivalent networks for TM and TE fields

be used in place of the Fourier transform and some mathematical manipulations are different. Once again, the resonant frequency, radiation Q and far field patterns have been numerically obtained.[18] The results agreed well with published data. Note that the results reported in References 17 and 18 are for relatively thin structures in order to compare the present results with those available in literature. However, as the operating frequency gets higher and the substrate becomes electrically thick, the present method is quite useful since all the field phenomena are included in the solution process unlike many other methods.

4. Review of Dielectric Waveguide Techniques

One book chapter on Dielectric Waveguide Type Millimeter Wave Integrated Circuits has been written under the support of the present grant and is being printed at this time.[19] An invited paper on dielectric waveguide techniques will be presented at 1981 IEEE MTT International Microwave Symposium in Los Angeles.[20]

5. Conclusions

In this report, we summarized the projects carried out under sponsorship of DAAG29-78-G-0145. Some problems included in this report will be investigated more deeply during the next contract period.

REFERENCES

1. M. V. Schneider, "Millimeter-wave integrated circuits," 1973 IEEE MTT International Microwave Symposium, Boulder, CO, June 1973.

2. T. Itoh, "Inverted strip dielectric waveguide for millimeter-wave integrated circuits," IEEE Trans. Microwave Theory Tech., Vol. MTT-24, pp. 821-827, Nov. 1976.

3. T. Itoh and B. Adelseck, "Trapped image guide for millimeter-wave circuits," IEEE Trans. Microwave Theory Tech., Vol. MTT-28, pp. 1433-1436, Dec. 1980.

4. T. Itoh and F.-J. Hsu, "Distributed Bragg reflector Gunn oscillators for dielectric millimeter-wave integrated circuits," IEEE Trans. Microwave Theory Tech., Vol. MTT-27, pp. 514-518, May 1979.

5. B. S. Song and T. Itoh, "Distributed Bragg reflection dielectric waveguide oscillators," IEEE Trans. Microwave Theory Tech., Vol. MTT-27, pp. 1019-1022, Dec. 1979.

6. T. Itoh and F.-J. Hsu, "Application of inverted strip dielectric waveguides for measurement of the dielectric constant of low-loss materials at millimeter-wave frequencies," IEEE Trans. Microwave Theory Tech., Vol. MTT-27, pp. 841-844, Oct. 1979.

7. C. Chang and T. Itoh, "Resonant characteristics of dielectric resonators for millimeter-wave integrated circuits," Archiv für Elektronik und Übertragungstechnik, Vol. 33, pp. 141-144, April 1979.

8. S. B. Cohn, "Slot line on a dielectric substrate," IEEE Trans. Microwave Theory Tech., Vol. MTT-17, pp. 768-778, Oct. 1969.

9. Y. Shih, J. Rivera and T. Itoh, "Directive planar excitation of an image-guide," 1981 IEEE MTT International Microwave Symposium, Los Angeles, CA, June 1981.

10. P. Yen, J. A. Paul and T. Itoh, "Millimeter-wave planar slot antennas with dielectric feeds," 1981 IEEE MTT International Microwave Symposium, Los Angeles, CA, June 1981.

11. T. Itoh, "Spectral domain immittance approach for dispersion characteristics of generalized printed transmission lines," IEEE Trans. Microwave Theory Tech., Vol. MTT-28, pp. 733-736, July 1980.

12. T. Ioth, "Generalized spectral domain method for multiconductor printed lines and its application to tunable suspended microstrips," IEEE Trans. Microwave Theory Tech., Vol. MTT-26, pp. 983-987, Dec. 1978.

13. L.-P. Schmidt and T. Itoh, "Spectral domain analysis of dominant and higher order modes in fin-lines," IEEE Trans. Microwave Theory Tech., Vol. MTT-28, pp. 981-985, Sept. 1980.

14. L.-P. Schmidt, T. Itoh and H. Hofmann, "Characteristics of unilateral fin-line structures with arbitrarily located slots," IEEE Trans. Microwave Theory Tech., Vol. MTT-29, April 1981.

15. L.-P. Schmidt and T. Itoh, "Characteristics of a generalized fin-line for millimeter-wave integrated circuits," Int. J. Infrared and Millimeter Waves, Vol. 2, May 1981.

16. B. S. Song and T. Itoh, "Comparison of distributed Gunn devices with microstrip and coplanar electrodes," Workshop on Compound Semiconductor Microwave Materials and Devices, San Francisco, CA, Feb. 1980.

17. T. Itoh and W. Menzel, "A full wave analysis method for open microstrip structures," IEEE Trans. Antennas and Propagation, Vol. AP-29, Jan. 1981.

18. K. Araki and T. Itoh, "Hankel transform domain analysis of open circular microstrip radiating structures," IEEE Trans. Antennas and Propagation, Vol. AP-29, Jan. 1981.

19. T. Itoh, "Dielectric waveguide type millimeter-wave integrated circuits," Chapter 5, Infrared and Millimeter Waves, Vol. 4, ed. K. Button, Academic Press, New York, NY, 1981.

20. T. Itoh, "Open guided wave structures for millimeter-wave circuits," (Invited) 1981 IEEE MTT International Microwave Symposium, Los Angeles, CA, June 1981.

LIST OF PERSONNEL

Principal Investigator

T. Itoh

Research Associates

L.-P. Schmidt
K. Araki
I. Awai

Research Assistants

B. S. Song
C. Chang
J. Rivera
Y. Shih
D. Parse

Research Student

D. C. Zimmermann

Degrees Awarded

D. C. Zimmermann, Master of Science, December 1979
J. Rivera , Master of Science, May 1980

LIST OF PUBLICATIONS

Book Chapter

1. T. Itoh, "Dielectric waveguide type millimeter-wave integrated circuits," Chapter 5, Infrared and Millimeter Waves, Vol. 4, ed. K. Button, Academic Press, New York, NY, 1981.

Journal Articles

1. T. Itoh, "Generalized spectral domain method for multiconductor printed lines and its application to tunable suspended microstrips," IEEE Trans. Microwave Theory Tech., Vol. MTT-26, pp. 983-987, December 1978.

2. C. Chang and T. Itoh, "Resonant characteristics of dielectric resonators for millimeter-wave integrated circuits," Archiv für Elektronik und Übertragungstechnik, Vol. 33, pp. 141-144, April 1979.

3. T. Itoh and F.-J. Hsu, "Distributed Bragg reflector Gunn oscillators for dielectric millimeter-wave integrated circuits," IEEE Trans. Microwave Theory Tech., Vol. MTT-27, pp. 514-518, May 1979.

4. T. Itoh and F.-J. Hsu, "Application of inverted strip dielectric waveguide for measurement of the dielectric constant of low-loss materials at millimeter-wave frequencies," IEEE Trans. Microwave Theory Tech., Vol. MTT-27, pp. 841-844, October 1979.

5. B. S. Song and T. Itoh, "Distributed Bragg reflection dielectric waveguide osiellators," IEEE Trans. Microwave Theory Tech., Vol. MTT-27, pp. 1019-1022, December 1979.

6. T. Itoh, "Spectral domain immittance approach for dispersion characteristics of generalized printed transmission lines," IEEE Trans. Microwave Theory Tech., Vol. MTT-28, pp. 733-736, July 1980.

7. L.-P. Schmidt and T. Itoh, "Spectral domain analysis of dominant and higher order modes in fin-lines," IEEE Trans. Microwave Theory Tech., Vol. MTT-28, pp. 981-985, September 1980.

8. T. Itoh and B. Adelseck, "Trapped image guide for millimeter-wave circuits," IEEE Trans. Microwave Theory Tech., Vol. MTT-28, pp. 1433-1436, December 1980.

9. T. Itoh and W. Menzel, "A high frequency analysis method for open microstrip structures," IEEE Trans. Antennas and Propagation, Vol. AP-29, January 1981.

10. K. Araki and T. Itoh, "Hankel transform domain analysis of open circular microstrip radiating structures," IEEE Trans. Antennas and Propagation, Vol. AP-29, January 1981.

11. L.-P. Schmidt, T. Itoh and H. Hofmann, "Characteristics of unilateral fin-line structures with arbitrarily located slots," IEEE Trans. Microwave Theory Tech., Vol. MTT-29, April 1981.

12. L.-P. Schmidt and T. Itoh, "Characteristics of a generalized fin-line for millimeter-wave integrated circuits," Int. J. Infrared and Millimeter Waves, Vol. 2, May 1981.

Conference Presentations

1. T. Itoh and F.-J. Hsu, "Application of inverted strip dielectric waveguides for measurement of material properties at millimeter-wave frequencies," European Microwave Conference, Paris, France, September 1978.

2. C. Chang and T. Itoh, "Spectral domain analysis of dominant and higher order modes in fin-lines," IEEE MTT International Microwave Symposium, Orlando, FL, May 1979.

3. B. S. Song and T. Itoh, "A distributed feedback dielectric waveguide oscillator with a built-in leaky-wave antenna," IEEE MTT International Microwave Symposium, Orlando, FL, May 1979.

4. T. Itoh, "Spectral domain immittance approach for dispersion characteristics of shielded microstrips with tuning septums," European Microwave Conference, Brighton, England, September 1979.

5. T. Itoh and W. Menzel, "A high frequency analysis method for open microstrip structures," Workshop on Printed Circuit Antenna Technology, Las Cruces, NM, October 1979.

6. T. Itoh and D. C. Zimmermann, "Characteristics of microstrip slot lines," National Radio Science Meeting, Boulder, CO, November 1979.

7. B. S. Song and T. Itoh, "Comparison of distributed Gunn devices with microstrip and coplanar electrodes," Workshop on Compound Semiconductor Microwave Materials and Devices, San Francisco, CA, February 1980.

8. T. Itoh and B. Adelseck, "Trapped image guide for millimeter-wave circuits," IEEE MTT International Symposium, Washington, D.C., May 1980.

9. L.-P. Schmidt, T. Itoh and H. Hofmann, "Characteristics of unilateral fin-line structures with arbitrarily located slots," IEEE MTT International Microwave Symposium, Washington, D.C., May 1980.

10. T. Itoh and B. Adelseck, "Trapped image guide leaky-wave antennas for millimeter-wave applications," IEEE AP-S International Symposium, Quebec, Canada, June 1980.

11. K. Araki, T. Itoh and Y. Naito, "Hankel transform domain analysis of open circular microstrip radiating structures," IEEE AP-S International Symposium, Quebec, Canada, June 1980.

12. T. Itoh and L.-P. Schmidt, "Characteristics of a generalized fin-line for millimeter-wave integrated circuits," International URSI Symposium, Munich, W. Germany, August 1980.

13. T. Itoh, "Millimeter waveguiding structures," Workshop on Modern Millimeter Wave Systems, Estes Park, CO, October 1980.

14. Y. Shih, J. Rivera and T. Itoh, "Directive planar excitation of an image-guide," IEEE MTT International Microwave Symposium, Los Angeles, CA, June 1981.

15. T. Itoh, "Open guided wave structures for millimeter-wave circuits," (Invited) IEEE MTT International Microwave Symposium, Los Angeles, CA June 1981.

16. P. Yen, J. A. Paul and T. Itoh, "Millimeter-wave planar slot antennas with dielectric feeds," IEEE MTT International Microwave Symposium, Los Angeles, CA, June 1981

APPENDIX 1

Distributed Bragg Reflection Dielectric Waveguide Oscillators

BANG-SUP SONG, STUDENT MEMBER, IEEE, AND TATSUO ITOH, SENIOR MEMBER, IEEE

Abstract—**Dielectric waveguide Gunn oscillators are presented in which the cavity consists of grating structures exhibiting either the surface-wave stopband or the leaky-wave stopband. Oscillation conditions and design criteria of the grating structures are studied. When a grating exhibiting the leaky-wave stopband is used in the oscillator, the extraction of the output power in the direction perpendicular to the dielectric waveguide axis is possible. This is because such a grating becomes a broadside-firing leaky-wave antenna with high input VSWR.**

I. Introduction

IN THIS PAPER, we present first a more detailed study of a distributed Bragg reflection (DBR) Gunn oscillator developed earlier [1]. Then we introduce a new DBR oscillator in which a leaky-wave antenna is integrated. These oscillators are made of dielectric waveguides and are believed useful for millimeter and microwave integrated circuits. The leaky-wave antenna integrated in the new structure is broadside firing. In conventional antenna applications, such a broadside condition is avoided due to its high VSWR characteristics. In the present work, however, this high VSWR is intentionally made use of for providing a frequency dependent positive feedback to the gain device in the oscillator.

In most dielectric waveguide millimeter-wave integrated circuits, a solid-state oscillator is made of a Gunn or IMPATT diode implanted in a rectangular dielectric waveguide cavity [2]. In such a structure, the Fresnel reflection from the end surfaces of the resonator provides feedback to the active device and leads to oscillation. In the recently developed original version of the DBR Gunn oscillators [1], however, the feedback is provided by the so-called surface-wave stopband phenomenon of the grating structures created in the dielectric waveguide [3]. As is also demonstrated in the band-reject filter [4], the surface wave is strongly reflected back from the grating structure in a narrow frequency region. Such a frequency sensitive reflection is useful for realizing a high-Q cavity for the oscillator made of a dielectric waveguide. In practice, the DBR oscillator resembles the DBR GaAs lasers developed in optics [5], [6].

It is well known that the stopband phenomenon appears not only in the surface wave, but also in the leaky-wave regions [7]. In the structures described in this paper, the leaky-wave stopband as well as the surface-wave stopband is used for providing positive feedback leading to oscillation. We will test an oscillator in which the grating on one side of the gain device provides a surface-wave stopband and the one on the other side gives a leaky-wave stopband. This leaky-wave structure also gives rise to the broadside radiation which facilitates easy output power extraction.

Manuscript received May 5, 1979; revised September 11, 1979. This work was supported in part by a U.S. Army Research under Grant DAAG29-78-G-0145.

The authors are with the Department of Electrical Engineering, the University of Texas, Austin, TX 78712.

II. Oscillator Design

It is known that Gunn devices exhibit negative differential conductance when the operating frequency is an integral multiple of transit frequency [8], [9]. Therefore, the negative conductance and the positive susceptance of the Gunn device peak around the transit frequency $f_t = \bar{v}/l$, where $\bar{v}$ is the average electron drift velocity and l is the diode length. Since the electron drift velocity depends on the applied field [10], however, it is possible to shift the peak of the negative conductance and the positive susceptance, as well as their amplitudes, by varying the bias voltage until the oscillation conditions in (1a) and (1b) are satisfied. These oscillation conditions are

$$G_d + G_l = 0 \tag{1a}$$

$$B_d + B_l = 0 \tag{1b}$$

where G_d and B_d are the conductance and the susceptance of the diode, and G_l and B_l are the conductance and the susceptance external to the diode. Around the transit frequency, the Gunn device can be represented by an equivalent circuit consisting of a negative conductance ($G_d < 0$) in shunt with a positive susceptance ($B_d > 0$) [11]. Therefore, we have to supply the diode externally with a negative susceptance which is inductive to satisfy the oscillation condition (1b).

Although various types of gratings can be used, mechanically created notch type periodic grooves in the dielectric waveguide have been used in the oscillators. For the surface-wave stopband, the period of grating d is chosen such that

$$\mathrm{Re}(\beta d) = \pi \tag{2}$$

where β is the phase constant of the dielectric waveguide with gratings. β can be approximated by the following dispersion relation [12]:

$$\cos\beta d = \cos(\beta_{e1} a)\cos[\beta_{x1}(d-a)] - \tfrac{1}{2}\left(\frac{\beta_{x1}}{\beta_{e1}} - \frac{\beta_{e1}}{\beta_{x1}}\right)\sin(\beta_{e1} a)\sin[\beta_{x1}(d-a)] \tag{3}$$

0018-9480/79/1200-1019$00.75 © 1979 IEEE

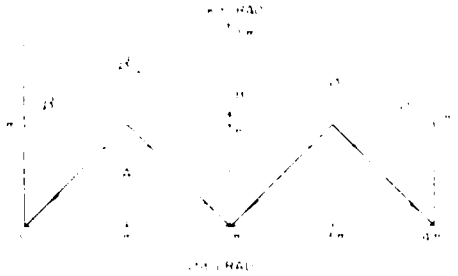

Fig. 1. kd–βd diagram of the grating structure; $\epsilon_r = 10$, $w = 5.6$ mm, $d = 11.0$ mm, $a = 5.5$ mm, $h = 3.0$ mm, $t = 0.9$ mm.

where β_G and β_{NG} are the phase constants in the grooved and nongrooved sections of the waveguide, respectively. In the stopband, β is complex due to mode coupling between the forward and backward waves. When we neglect this mode coupling, the dispersion curve (kd βd diagram) will look like the one shown in Fig. 1. Point $A(\beta d = \pi)$ corresponds to the surface-wave stopband where strong mode coupling occurs between the two space harmonics β_0 and $-\beta_1$ (negative β means traveling backward). All of these space harmonics are interrelated via

$$\beta_m = \beta_0 + \frac{2m\pi}{d}, \qquad m = 0, 1, 2, \cdots \tag{4}$$

where β_0 is the phase constant of the dominant ($m = 0$) space harmonic.

The leaky-wave stopband is created at $\beta d = 2\pi$ (Point B in Fig. 1) by the interaction between the space harmonics β_0 and $-\beta_2$ which are no longer surface waves, and the radiation peak is in the broadside direction normal to the waveguide surface. This leaky-wave stopband gives strong reflection due to the backward space harmonic $-\beta_2$ being coupled to β_0, which results in high VSWR.

The original version of the DBR oscillator employing a surface-wave stopband can be implemented as in Fig. 2 by placing a Gunn device in a small vertical hole drilled in a dielectric image guide [1]. The ground plane is used as a heat sink as well as a dc bias return for the device. The bias is supplied through a thin wire connected to the positive terminal of the diode. The equivalent circuit of the DBR Gunn oscillator in Fig. 2 can be drawn as in Fig. 3(a) [1], [2], where Y_d is the equivalent admittance of the diode, and Y_1, Y_2 are the input admittances looking into the two grating reflectors on both sides. These grating reflectors are capacitive in the stopband. Thus a quarter-wave transformer is introduced between the diode and the reflector to provide an inductive load to the device. The resulting simplified equivalent circuit is shown in Fig. 3(b) and Fig. 3(c) when we have made use of the following relations.

$$Y_e = Y_0^2\left(\frac{1}{Y_1} + \frac{1}{Y_2}\right) = G_e + jB_e$$

$$Y_d = G_d + jB_d \tag{5}$$

where Y_e is the total equivalent admittance of the external

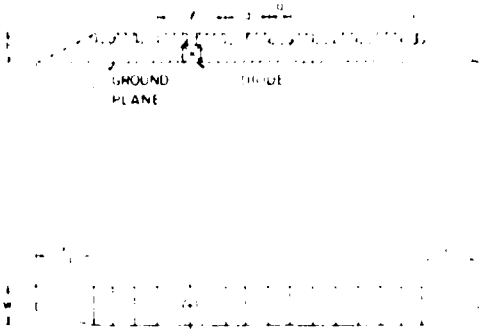

Fig. 2. An original version of the DBR oscillator structure. $\epsilon_r = 10$, $h = 3.0$ mm, $l = 16.5$ mm, $d = 11.0$ mm, $a = 5.5$ mm, $w = 5.6$ mm, $t = 0.9$ mm, $t_1 = 16.0$ mm, $t_2 = 11.5$ mm.

Fig. 3. Equivalent circuit of the DBR oscillator.

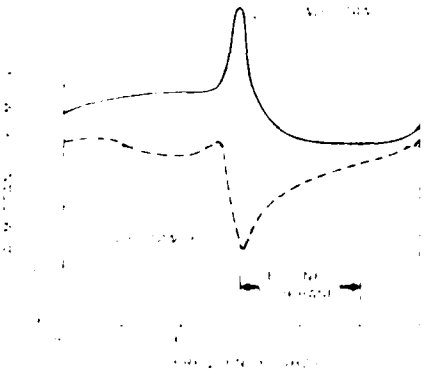

Fig. 4. Admittance external to the diode in the Fig. 2 structure.

reflectors. The variation of Y_e with frequency is shown in Fig. 4 for the DBR oscillator in Fig. 2. The conductance and the susceptance peak at the lower edge of the designed stopband. Even though we cannot determine exactly the values of G_d and B_d of the Gunn device, G_d and B_d can be controlled up to a few millimhos by the external bias voltage as mentioned earlier in this section. Another important factor which cannot be neglected is the shunt capacitance and the series inductance of the commercial diode packaging which are approximately in the range of a few tenths of a picofarad or nanohenry, respectively. At

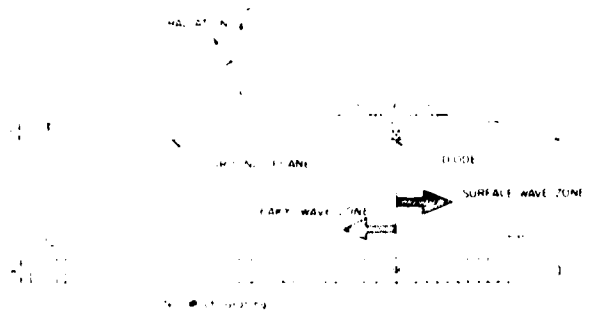

Fig. 5. Structure of a new DBR oscillator with a built-in leaky-wave antenna; $N=10$, $\epsilon_r=10$, $l=22.0$ mm, $d=11.0$ mm, $a=4.0$ mm, $w=6.0$ mm, $t=0.9$ mm, $h=3.0$ mm, $t_1=12.0$ mm, $t_2=4.0$ mm, $t_3=19.0$ mm.

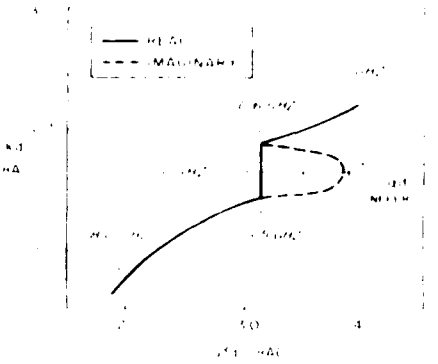

Fig. 6. Detailed kd-βd diagram around the point A in Fig. 1.

10 GHz, these correspond to 10~40 mho. Therefore, when we consider this effect, oscillations are likely to occur in the lower half of the stopband where the admittance peak is located. So it is better to design the center frequency of the stopband a little higher than the desired operating frequency.

The new DBR oscillator using the high VSWR leaky-wave stopband is shown in Fig. 5. In this structure, the left-hand side of the Gunn diode provides a dual function. It provides the reflection for oscillation as well as the broadside radiation for the antenna. The period of grating on the left is about two times that of the surface-wave structure on the right, viz., $\mathrm{Re}(\beta d)\cong 2\pi$ on the left-hand side and $\mathrm{Re}(\beta d)=\pi$ on the right. The radiation angle from the leaky-wave structure can be determined by [4], [13]

$$\theta=\pm\sin^{-1}\left[\frac{\mathrm{Re}(\beta_{-1})}{k}\right] \tag{6}$$

where θ is the angle measured from the direction normal to the surface and k is the free-space wavenumber. At the leaky-wave stopband (Point B), $\mathrm{Re}(\beta d)\approx 2\pi$ which means a radiation angle of $\theta\approx 0$ (broadside). This angle varies slightly depending on the oscillation frequency.

The reflection phenomenon due to the stopband is frequency sensitive, and the bandwidth and reflection depend on the grating profile, the length of the grating region, etc. In this work, bandwidth has been made wide (1 GHz) so that the oscillation can be easily attained.

III. Results and Discussions

Although we can provide the design at much higher millimeter-wave frequencies, we have selected X band for design and demonstration. This is due to better availability of measurement equipment and greater ease of experimental procedures. After the feasibility of our new concepts is demonstrated, we can go to higher frequencies in the future.

The dielectric waveguides are made of a synthetic dielectric material, Custom HiK ($\epsilon_r=10$). The number of grating elements can be determined by the required magnitude of the feedback. We can calculate the amount of feedback from (3), and the imaginary part of β plotted in Fig. 6 explains the feedback mechanism in the stopband

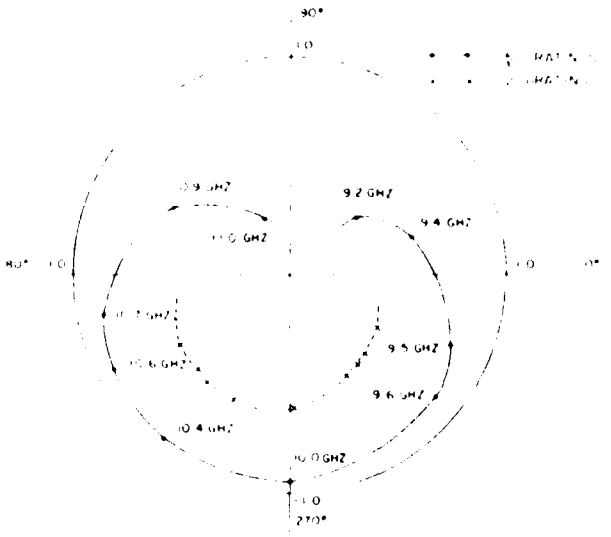

Fig. 7. Reflection coefficient of 5- and 2-element gratings in dielectric waveguide in Fig. 2.

[3], [5], [6]. Fig. 7 shows the surface-wave reflection coefficients of a 5- and 2-element notch-type grating on the dielectric waveguides. Groove depth and grating period are adjusted so as to give a 10-GHz center frequency and a 1-GHz bandwidth. The reflection coefficient at 10 GHz is found to be 0.95 in the 5-element grating, but in the 2-element grating, the reflection coefficient at 10 GHz reduces to 0.63. The latter may be useful for the output port of the original DBR oscillator shown in Fig. 2 in which the far end of each grating is tapered to avoid unwanted end reflection. Even though we design the stopband which spans from 9.5 to 10.5 GHz, oscillation frequencies will be lower than the 10-GHz center frequency as mentioned in Section II. Oscillation frequencies and power output were observed by varying the bias voltage of the Gunn device in the DBR oscillator shown in Figs. 2 and 5. The results are plotted in Figs. 8 and 9. Oscillation frequencies measured were predominantly in the lower half of the stopband (9.5~10.0 GHz). The power was measured by receiving the radiation from one end of the resonator.

In the new DBR oscillator with a built-in leaky-wave antenna, with bias voltage of 7 V, the resonant frequency

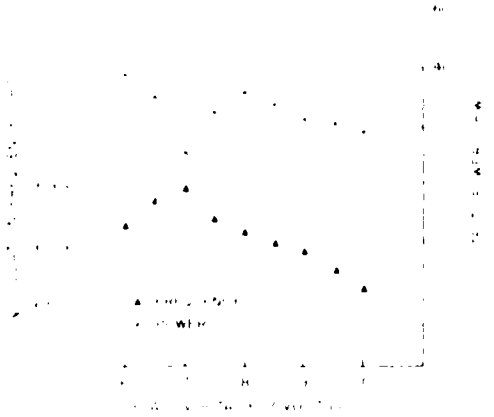

Fig. 8. Measured oscillation characteristics of the oscillator in Fig. 2

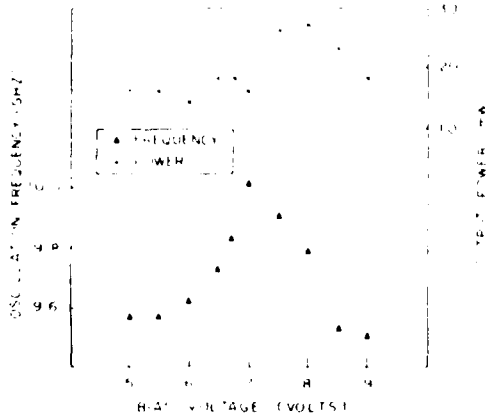

Fig. 9. Measured oscillation characteristics of the oscillator in Fig. 5.

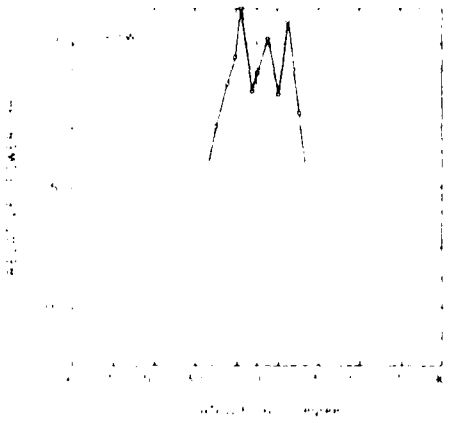

Fig. 10. Broadside radiation pattern from the DBR oscillator in Fig. 5.

was observed around 9.995 GHz, and the measured broadside radiation is shown in Fig. 10. When measuring the radiation pattern, the radiation from the diode was properly shielded.

It is conjectured that the split of the main lobe is caused by several factors. One is the poor spectral purity which is not an inherent phenomenon of this type of oscillator but is rather due to our intentional broad-band design of the cavity. Another is the strong mode coupling between the forward and backward space harmonics in the leaky wave region which have different radiation angles.

IV. Conclusions

We have presented studies of DBR Gunn oscillators with surface-wave and leaky-wave stopbands and some results for these oscillator structures. The structure is believed to give versatility in designing millimeter-wave integrated circuits. Further works need to be carried out to obtain spectral purity and better frequency control especially for the structures with an integrated leaky-wave antenna. It is possible to design grating structures with a much narrower bandwidth for more stable oscillation. In designing the oscillator, it is advisable to place the operating frequency in the lower half of the stopband. It is also required to insert quarter-wave transformer between the device and the grating reflector. Mechanical perturbation may be incorporated for adjusting the device impedance for possible tuning of frequency and/or power.

References

[1] T. Itoh and F. Hsu, "Distributed Bragg reflector Gunn oscillators for dielectric millimeter-wave integrated circuits," *IEEE Trans. Microwave Theory Tech.*, vol. MTT-27, pp. 514–518, May 1979.

[2] H. Jacobs, G. Novick, C. M. LoCascio, and M. M. Chrepta, "Measurement of guided wavelength in rectangular dielectric waveguides," *IEEE Trans. Microwave Theory Tech.*, vol. MTT-24, pp. 815–820, Nov. 1976.

[3] S. T. Peng, T. Tamir, and H. L. Bertoni, "Theory of periodic dielectric waveguides," *IEEE Trans. Microwave Theory Tech.*, vol. MTT-23, pp. 123–133, Jan. 1975.

[4] T. Itoh, "Application of gratings in a dielectric waveguide for leaky-wave antennas and band-reject filters," *IEEE Trans. Microwave Theory Tech.*, vol. MTT-25, pp. 1134–1138, Dec. 1977.

[5] S. Wang, "Principles of distributed feedback and distributed Bragg reflection lasers," *IEEE J. Quantum Electron.*, vol. QE-10, pp. 413–427, Apr. 1974.

[6] W. Streifer, D. R. Scifres, and R. D. Burnham, "Coupled wave analysis of DFB and DBR lasers," *IEEE J. Quantum Electron.*, vol. QE-13, pp. 134–141, Apr. 1977.

[7] R. E. Collins, F. J. Zucker, and A. Hessel, *Antenna Theory*. New York: McGraw-Hill, 1969, pt. II, ch. 19.

[8] S. M. Sze, *Physics of Semiconductor Devices*. New York: Wiley, 1969, ch. 14.

[9] D. E. McCumber and A. G. Chynoweth, "Theory of negative conductance amplification and of Gunn instabilities in two-valley semiconductors," *IEEE Trans. Electron Devices*, vol. ED-13, pp. 4–21, Jan. 1966.

[10] P. N. Robson, G. S. Kino, and B. Fay, "Two-Port microwave amplification in long samples of gallium arsenide," *IEEE Trans. Electron Devices*, vol. ED-14, pp. 612–615, Sept. 1967.

[11] H. W. Thim, "Linear microwave amplification with Gunn oscillators," *IEEE Trans. Electron Devices*, vol. ED-14, pp. 517–522, Sept. 1967.

[12] R. E. Collin, *Foundations for Microwave Engineering*. New York: McGraw-Hill, 1966, ch. 8.

[13] K. L. Klohn, R. E. Horn, H. Jacobs, and E. Freibergs, "Silicon waveguide frequency scanning linear array antenna," *IEEE Trans. Microwave Theory Tech.*, vol. MTT-26, pp. 764–773, Oct. 1978.

APPENDIX 2

Application of Inverted Strip Dielectric Waveguides for Measurement of the Dielectric Constant of Low-Loss Materials at Millimeter-Wave Frequencies

TATSUO ITOH, SENIOR MEMBER, IEEE, AND FWU-JIH HSU, MEMBER, IEEE

***Abstract*—An entirely new method for measuring dielectric properties of slab-type materials is developed by using a novel dielectric waveguide structure originally designed for millimeter-wave integrated circuits. The method entails the measurement of the stopband of the grating structure created in the dielectric waveguide. Several examples of measurement results are reported.**

I. Introduction

With increasing use of dielectric resonators [1], dielectric waveguides [2], and printed transmission lines at higher frequencies, simple methods for accurately predicting the properties of dielectric materials become very important. There are currently a number of methods available for measuring dielectric properties of material media at microwave and millimeter-wave frequencies. One typical method is the use of waveguides or waveguide cavities, which are either partially or completely filled with dielectric materials to be measured [3]. Cavities made of striplines or microstrip lines have also been used [4], [5]. In free-space environment, scattering of electromagnetic energy from a dielectric sphere can be used for evaluating the dielectric property of the sphere [6].

The paper proposes a novel approach to measurement of dielectric constants of low-loss slab materials at microwave and millimeter-wave frequencies. The method makes use of stopband phenomena observed in periodic structures created in an inverted strip dielectric (IS) waveguide developed recently [7]. The principle of the measurement process will be explained in the following paper.

II. Principle of Measurement

The cross section of the IS waveguide is shown in Fig. 1(a). The major portion of the wave energy propagates in that portion of the guiding layer immediately above the dielectric strip [2]. When periodic grooves are created in the strip as shown in Fig. 1(b), the propagation characteristic of the IS waveguide is periodically modulated and a grating structure is created. Depending on the electrical length of the grating period d, the structure works either as a leaky-wave antenna or a band-reject filter [7].

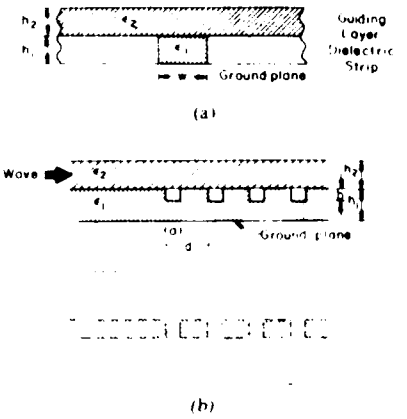

Fig. 1. Experimental setup. (a) Cross section. (b) Side and top views.

Although the antenna scheme may be used it is not as practical as the filter structure as the field measurement is required. Hence, we will use the filter method in this paper. The frequency response of the filter is a function of all the dimensions of the IS waveguide, the grating period, profile of the grating, and the dielectric constants of the materials involved. Hence, if one measures the frequency response of the filter, the dielectric constant of one of the materials may be determined provided all other parameters are known.

If we use a bandstop filter scheme, it is possible to find out the dielectric constant of one of the materials in the waveguide by simply measuring the frequency related to the stopband, such as the center frequency, the lower band edge, or the upper band edge.

In the proposed measurement setup, we use a slab material with unknown dielectric constant as the guiding layer of the IS waveguide. The periodic grooves are

Manuscript received December 26, 1978; revised June 4, 1979. This work was supported in part by a U.S. Army Research Grant DAAG29-78-G0145. The major portion of this paper was presented at the European Microwave Conference, Paris, France, in September 1978.

T. Itoh is with the Department of Electrical Engineering, The University of Texas, Austin, TX 78712.

F. J. Hsu is with the Anaconda Telephone Company, Anaheim, CA 92801.

0018-9480/79/1000-0841$00.75 © 1979 IEEE

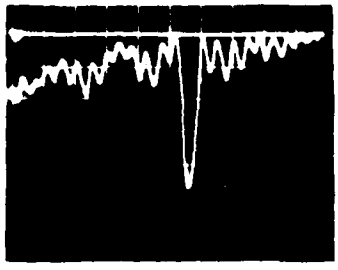

Fig. 2. Typical sweep response from the grating structure. 20 mV/div. 12.4–18 GHz.

created as shown in Fig. 1 in the dielectric strip which has a known dielectric constant. When we excite this structure with a sweep source a strong reflection is observed at the stopband, provided the frequency range of the sweeper covers the stopband. A typical response from an IS waveguide with periodic grooves in its dielectric strip is shown in Fig. 2.

Let us now discuss the algorithm to obtain the dielectric constant from the measured data. First, if we assume that the dielectric constant ϵ_2 of the guiding layer is known, the center frequency f_c of the stopband is given by

$$f_c = F(h_1, h_2, \epsilon_1, w, d, a, b, \epsilon_2) \tag{1}$$

where h_1, w, and ϵ_1 are the thickness, width, and dielectric constant of the dielectric strip, h_2 is the thickness of the guiding layer, and d is the grating period. Also, a and b are the length and the depth of the grooves. F indicates that f_c is a function of all the parameters in the parentheses. No closed form of F is available. However, values of f_c are given numerically, as explained in the Appendix.

Our problem at hand is to solve (1) for ϵ_2, that is, to obtain

$$\epsilon_2 = F^{-1}(h_1, h_2, \epsilon_1, w, d, a, b, f_c) \tag{2}$$

Since there is no closed form expression for (1), its inversion (2) does not have an analytical form either. However, we may use either a graphical method or a computer-optimization technique to accomplish the solution for ϵ_2. In the graphical method, a number of curves for f_c versus ϵ_2 are generated numerically from (1) for a number of structural parameters. Examples of curves are presented in Fig. 3. Once these curves are available, it is possible to obtain ϵ_2 graphically from the measured value of f_c for a corresponding set of structural parameters. For structures not provided with curves some interpolation procedures may be used.

Computer-optimization techniques, though more time consuming, generally provide more accurate answers than the graphical method. In such a method, a subroutine to perform numerical solutions of (1) is used repeatedly for an assumed value of ϵ_2 until the computed value of f_c becomes virtually identical to the measured f_c. This iteration scheme is carried out in a systematic manner, and the final assumed value of ϵ_2 is considered as that of the unknown material.

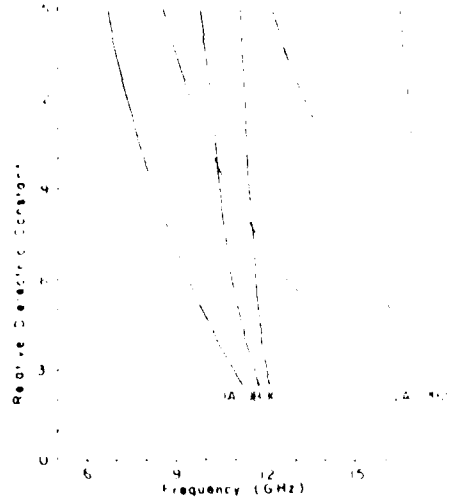

Fig. 3. Calculated results for stopband frequency f_c versus relative dielectric constant. h_2 is the thickness of the dielectric slab. d is the period of the grating. $h_1 = 6.35$ mm, $w = 16$ mm, $a = 1.59$ mm, $b = 3.16$ mm, $\epsilon_1 = 2.1$ (Teflon).

(1A) $h_2 = 6.35$ mm $\quad d = 10$ mm.
(1B) $h_2 = 3.175$ mm $\quad d = 10$ mm.
(1C) $h_2 = 1.5875$ mm $\quad d = 10$ mm.
(2A) $h_2 = 6.35$ mm $\quad d = 6.25$ mm.
(2B) $h_2 = 3.175$ mm $\quad d = 6.25$ mm.
(2C) $h_2 = 1.5875$ mm $\quad d = 6.25$ mm.

III. Measurement Procedures

The IS waveguide with grating sections can be assembled from a large ground plane, a rectangular dielectric strip (ϵ_1) with periodic grooves, and a slab material to be measured which is used as the guiding layer. It is helpful in practice if the period of grooves is determined in such a way that the stopband appears in the frequency range where the field is well guided in the IS waveguide with the guiding layer made of a commonly used material such as fused quartz. Each component is securely positioned by mechanical pressure between the guiding layer and the ground plane by means of clamps located away from the waveguiding portion. Since any air gap between dielectric materials themselves and the ground plane may be a potential source of error in the final results, smooth dielectric surfaces and relatively strong mechanical pressure are essential. In order to excite the IS waveguide assembly efficiently and to resolve the stopband clearly, a good transition from the conventional rectangular metal waveguide to the assembly is important. We have accomplished this requirement by the use of a tapered rectangular dielectric waveguide. The pointed end of the tapered structure is inserted into the rectangular metal waveguide which is connected to a microwave sweep source by way of a reflectometer setup. The other end of the tapered section is flat and butt jointed to the end surface of the slab material immediately above the dielectric strip (ϵ_1).

The measurement procedure is as follows. 1) First obtain a sweep response which is the ratio of the input

TABLE I
EXAMPLES OF MEASURED DIELECTRIC CONSTANTS

power to and the reflected power from the IS waveguide assembly. The range of sweep is adjusted until the stopband appears. Read the center frequency f_c of the stopband. Measure all the pertinent physical dimensions involved. 2) By using either a graphical method or a computer-optimization algorithm explained earlier, obtain the dielectric constant ϵ_2 of the unknown slab material.

IV. Results and Discussions

To demonstrate the validity of the method, several measurements have been performed in the frequency range up to 18 GHz. Although there is no inherent limit in frequency, we could not use any higher frequency due to unavailability of sweeper sources higher than 18 GHz. Examples of measured results are listed in Table I. It is seen that the results obtained in the present method are quite accurate. Note that for these examples we used a computer-optimization algorithm for inversion of (1).

We will now summarize some of the features of the present method.

1) Since the quantity to be measured is the frequency, the error involved in the measurement process itself is small.

2) The method is simple to use and the material to be measured can be easily replaced in the setup since the IS waveguide assembly, including the grating section, is held in position by applying the mechanical pressure between the guiding layer (unknown material) and the ground plane by means of clamps at the location away from the waveguiding portion.

3) The dissipation factor cannot be measured in the present setup. If the attenuation due to the material loss can be isolated, such a factor could be measured. However, in most open structures, it is extremely difficult to separate the radiation loss and material loss.

4) The accuracy of the methods depends on the inversion scheme of the measured data. For instance, both, the method to obtain β_{x_1} and β_{x_2} and the one for β by using (A1) are approximate, although they are usually quite accurate for the types of structures used here. Another problem is the convergence of the optimization routine. Sometimes, the convergence could be slow and one may be advised that the use of graphical method to obtain initial value in the optimization routine could be helpful.

The method proposed here does not replace other existing methods, in many of which both real and imaginary parts can be measured. Rather, the present method provides a simple alternative when only the real parts of dielectric constants in low loss materials are needed.

V. Conclusions

We proposed a simple method for measuring the dielectric constant of slab-type materials for microwave and millimeter-wave applications. A number of features of the method are listed as well as results of some example measurements. The latter agreed well with data supplied by manufacturers.

Appendix
Derivation of Equation (1)

Although a more exact analysis may be done, we present here a simple method to obtain the dispersion relation in the grating section in the IS waveguide operated in the surface-wave region. We will model the grating section as periodically cascaded transmission line. The complex phase constant β can be approximated in a manner similar to the one found in [8]. Each unit cell of the grating consists of two transmission lines; the grooved section of length a and the nongrooved section of length $(d - a)$. In this analysis, any junction susceptance between these two transmission lines will be neglected.

We will write the $ABCD$ matrix for each transmission-line section, and subsequently obtain the $ABCD$ matrix for the unit cell. Since the input and output signals of the unit cell differs only by a certain complex phase β, we obtain an eigenvalue equation for β, which is

$$\cos\beta d = \cos(\beta_{x_1} a)\cos\left[\beta_{x_2}(d-a)\right] - \frac{1}{2}\left(\beta_{x_1}/\beta_{x_2} + \beta_{x_2}/\beta_{x_1}\right) \cdot \sin(\beta_{x_1} a)\sin\left[\beta_{x_2}(d-a)\right] \quad \text{(A1)}$$

where β_{x_1} and β_{x_2} are the phase constants in the grooved and nongrooved sections of the IS waveguide. In the stopband $\beta d = \pi - j\alpha d$, where α is the attenuation constant caused by the mode coupling between space harmonics. The center frequency f_c is where α becomes a maximum.

The phase constants β_{x_2} and β_{x_1} can be obtained by solving the eigenvalue problems associated with the IS waveguides with or without a gap between the guiding layer (ϵ_2) and the dielectric strip (ϵ_1). The details of the derivation of β_{x_2} are given in [2]. To obtain β_{x_1}, we need to modify the method in [2] so that the air region between the guiding layer and the dielectric strip is taken appropriately into account. We need to modify eq. (3) in [2] and write an expression for the air-gap region. Obviously, the effective dielectric constant in such a region is different from the no-air-gap portion and, hence, eqs. (4) and (5) in [2] should be modified. However, all the remaining procedures in [2] remain unchanged for derivation of β_{x_1}.

The center frequency f_c can be computed in the following manner. First for a given set of structural and material parameters, we compute β_{x_2} and β_{x_1} versus frequencies. Then (A1) is solved for β, and we obtain f_c at which α becomes maximum.

References

[1] P. Guillon and Y. Garault, "Accurate resonant frequencies of dielectric resonators," *IEEE Trans. Microwave Theory Tech.*, vol. MTT-25, pp. 916–922, Nov. 1977.

[2] T. Itoh, "Inverted strip dielectric waveguide for millimeter-wave integrated circuits," *IEEE Trans. Microwave Theory Tech.*, vol. MTT-24, pp. 821–827, Nov. 1976.

[3] H. E. Stinehelfer, Sr., "Ridge waveguide resonant cavity for measuring dielectric constants," patent gazette, 3 384 814, May 21, 1968.

[4] L. S. Napoli and J. J. Hughes, "A simple technique for the accurate determination of the microwave dielectric constant for microwave integrated circuit substrates," *IEEE Trans. Microwave Theory Tech.*, vol. MTT-19, pp. 664–665, July 1971.

[5] T. Itoh, "A new method for measuring properties of dielectric materials using a microstrip cavity," *IEEE Trans. Microwave Theory Tech.*, vol. MTT-22, pp. 572 and 576, May 1974.

[6] J. S. Yu, J. Peter, Jr., and D. A. Castello, "A refractive index chart for a scattering sphere," *IEEE Trans. Antennas Propagat.*, vol. AP-18, pp. 75–83, Jan. 1970.

[7] T. Itoh, "Application of gratings in a dielectric waveguide for leaky-wave antennas and band reject filters," *IEEE Trans. Microwave Theory Tech.*, vol. MTT-25, pp. 1134–1138, Dec. 1977.

[8] R. E. Collin, *Foundation for Microwave Engineering*. New York: McGraw-Hill, 1966, ch. 8.

APPENDIX 3

Trapped Image Guide for Millimeter-Wave Circuits

TATSUO ITOH, SENIOR MEMBER, IEEE, AND BERND ADELSECK

Abstract—A novel dielectric waveguide is proposed for use in millimeter-wave integrated circuits, and a simple analysis for dispersion characteristics is developed. Numerical results agree reasonably with measured data. Radiation losses of this waveguide at curved sections are proven to be considerably less than those of the image guide. As an application of this waveguide, a leaky-wave radiator has been tested.

I. Introduction

RECENTLY, a number of works have been reported on millimeter-wave integrated circuits based on dielectric waveguides [1], [2]. In addition to image guide structures, several new waveguides have been proposed and tested [1], [3], [4]. An inherent problem of dielectric waveguides is the loss due to radiation at curved sections, junctions and discontinuities. This problem may be alleviated by the use of materials with high permittivities. However, use of such materials is often prohibited due to operating frequencies, sizes, and so on.

This paper proposes a new type of open dielectric waveguide which reduces the radiation loss at curved sections in dielectric integrated circuits. The structure is called a trapped image guide and is essentially a rectangular dielecric rod placed in a metal trough. The cross section of the trapped image guide is depicted in Fig. 1. In integrated circuit applications, almost all the bends are in the sideward direction. In ordinary image guides, the electromagnetic energy escapes from the guide as a propagating wave in the sideward direction at the bend. In the trapped image guide, such a leakage will be mostly reflected back to the dielectric portion by the metal walls if their height (the depth of the trough) h is reasonably large. As long as the waveguide is operated in the single mode region, the reflected energy will couple to the guided mode once again. Of course, an excessively large h is not very practical in actual integrated circuit applications. The trough may be readily created by machining a metal plate. An alternative is to machine a trough in a dielectric material followed by a metal plating.

Actual *Ka*-band (26.5–40 GHz) test setups of straight and curved sections of trapped image guide are photographed in Fig. 2. In these setups, instead of a machined trough, we added metal side walls to the ground plane for an image guide. Metal side walls to create the trough may be removed when an image guide setup is desired. Two transitions are provided for connecting the setups to conventional rectangular metal waveguides. Each of these transitions includes a semiconical horn originally designed for image guides (Fig. 2 without side walls) and tapers on the metal side walls to provide smooth transition to the trapped image guide. In what follows, we provide an approximate theoretical analysis of waveguiding char-

Fig. 1. Cross section of the trapped image guide

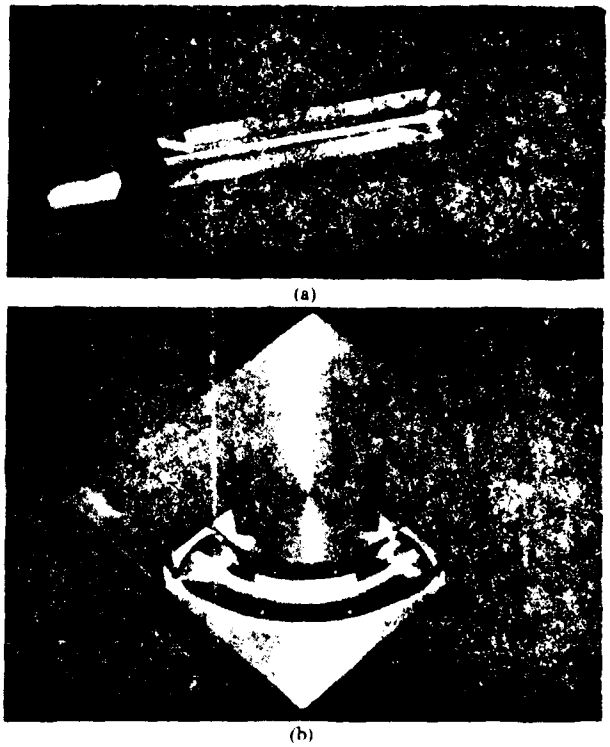

(a)

(b)

Fig. 2. Trapped image guide structures.

Manuscript received May 16, 1980. This work was supported by the U.S. Army under Research Grant DAAG29-78-G-0145.

T. Itoh is with the Department of Electrical Engineering, The University of Texas at Austin, Austin, TX 78712.

B. Adelseck is with AEG-Telefunken, Hoch-frequenztechnik D-7900, Ulm, West Germany

0018-9480/80/1200-1433$00.75 © 1980 IEEE

acteristics in the trapped image and the results are compared with experimental data. Some experimental investigations on the radiation loss characteristics at the bend are reported. An application of this waveguide as a frequency-scannable leaky-wave radiator is included.

II. Analysis of the Propagation Characteristics

The complete field components in the straight section of this waveguide may be derived from two field components

$$E_x = \frac{1}{\epsilon_r(y)}\left(\beta^2 - \frac{\partial^2}{\partial x^2}\right)\phi^e \tag{1}$$

$$H_x = \left(\beta^2 - \frac{\partial^2}{\partial x^2}\right)\phi^h \tag{2}$$

where ϵ_r is the relative dielectric constant in each constituent region in Fig. 1, β is the propagation constant, and ϕ^e and ϕ^h are two scalar potentials. Since the structure is very similar to the image guide, we classify guided modes into E^y and E^x types. In the former E_y and H_x are predominant field components and we neglect H_y by setting $\phi^h = 0$. Next, we assume that the metal wall height h is reasonably large and the electromagnetic wave is reasonably well guided. Then, it is possible to neglect the fields in Regions 7 and 8 in Fig. 1. This assumption allows us to mathematically increase h to infinity. When this is done, we can divide the cross section into three vertical regions: 3 and 5, 1 and 2, and 4 and 6. We will apply the method of effective dielectric constants (EDC) to this hypothetical structure [3], [4]. The EDC, ϵ_{eD} of the central region (1 and 2) for the vertically polarized (E^y) modes, may be obtained from

$$\epsilon_{eD} = \epsilon_r - \left(\frac{k_x}{k_0}\right)^2 \tag{3}$$

where k_x is the solution to the eigenvalue equation

$$\frac{k_x}{\epsilon_r}\tan k_x b - \sqrt{(\epsilon_r - 1)k_0^2 - k_x^2} = 0. \tag{4}$$

Equation (4) is obtained by matching $H_x \sim \phi^e$ and $E_z \sim (1/\epsilon_r(y))\partial\phi^e/\partial y$ at the interface $y = b$ for a hypothetical slab structure realized by letting a approach infinity. The EDC's for 3 and 5, and 4 and 6 regions are assumed to be one.

Next, we replace the hypothetical structure with another hypothetical one, consisting of a vertical slab of width $2a$ and dielectric constant ϵ_{eD} sandwiched between air regions of width c which are in turn terminated by vertical metal walls at $x = \pm(a+c)$. Notice that we now have a vertical two dimensional structure which is closed in the sideward direction. By solving the eigenvalue equation of this final hypothetical structure for the phase constant k_x in the slab region, we obtain the propagation constant of the guided mode from

$$k_z = \sqrt{\epsilon_{eD}k_0^2 - k_x^2}. \tag{5}$$

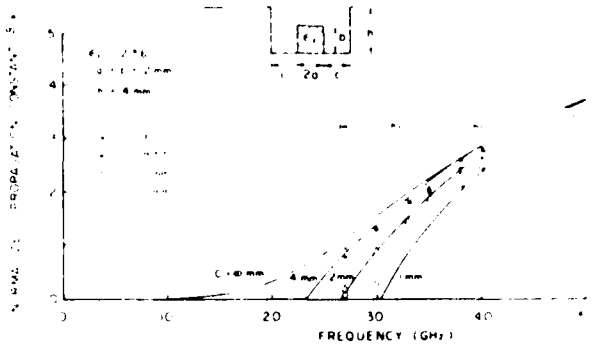

Fig. 3. Theoretical and experimental dispersion characteristics.

The method presented above is only an approximation. It is expected that the results are accurate at higher frequencies where the field is well guided. However, at lower frequencies, the results are less accurate because then the field extends to the Regions 7 and 8, and the assumption that h is infinite no longer applies.

Some numerical results are plotted in Fig. 3 on which experimental data are also indicated. In the computation, the value of c was varied and dispersion characteristics calculated. Also, the results for the ordinary image guide ($c \to \infty$) are included. It is noticed that all the results for the trapped image guide approach those for the image guide at higher frequencies because most of the energy is in the dielectric rod and the effect of the side walls becomes smaller. At lower frequencies the effect of the walls becomes significant. The propagation constant β approaches the cutoff value (free space wavelength k_0) faster than the image guide case. The smaller the value of c, the more pronounced the effect of the walls is. Actually, it is expected that the true value of β should be larger than the computed one near the cutoff, because there our assumption that h is infinite no longer holds. Such is clearly indicated by comparison between computed and experimental results for $c = 1$-mm case in the 25~30-GHz range. We also notice that all other experimental data qualitatively agree well with theoretical prediction. The experimental results at higher frequencies and those for image guides have some quantitative discrepancy with computed data. It is believed that the cause is in the experimental process which is quite sensitive to the perturbations applied to create standing wave patterns used to measure the guide wavelength.

Experimental results for transmission loss of a straight section of the waveguide are plotted in Fig. 4. The results include the loss and reflection at two transitions, each on both ends of the trapped image guide; one from the conventional metal waveguide to the image guide and another from the image guide to the trapped image guide. From Figs. 3 and 4, we find that the propagation characteristics are almost unaffected by the trough over 27~40 GHz if $c = 4$ mm. For smaller c values, the transmission loss increases at lower frequencies. This is because of larger scattering at transitions due to larger differences in

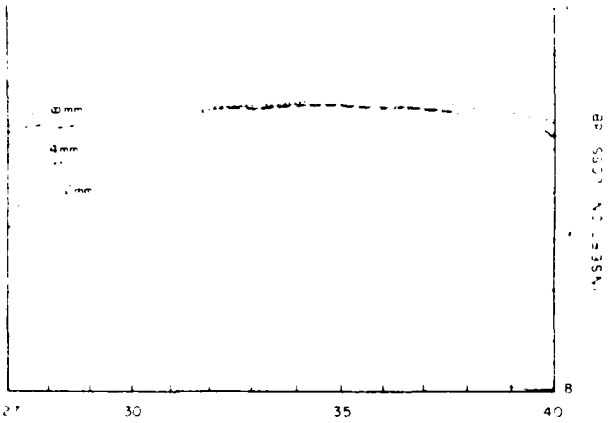

Fig. 4. Transmission loss in trapped image guides: the length between the transitions is 20 cm.

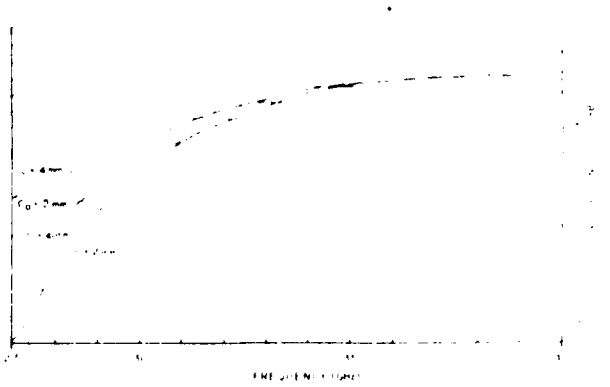

Fig. 5. Transmission loss in a curved section of the trapped image guide.

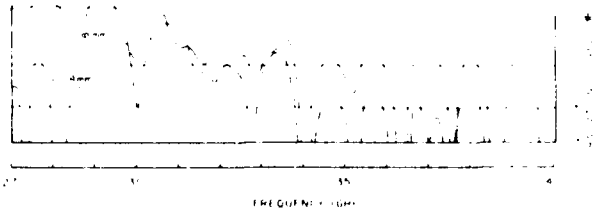

Fig. 6. Radiation loss from a curved section of the trapped image guide.

β between the image and trapped image guides. The scattering loss is largely in the form of radiation at the transition. However, no radiation has been detected from the trapped image guide section for any value of c.

III. Radiation at Curved Sections

Next, we investigated characteristics of a curved section of the trapped image guide. As an example, we used a 90° bend of center radius 63.7 mm (Fig. 2(b)). The launchers from the metal to image guides are identical to the ones used for the measurement of the straight section. Similarly tapered transitions are used from the image guide to the trapped image guide. We studied the following setups: an image guide ($c \to \infty$) and trapped image guides of $c = 2$ and 4 mm. In the two latter cases, we also removed the inside walls of the trap, as we believe the radiation at the bend is generally directed to the outer side, or away from the center of the curvature. These two structures are labeled with a subscript a, such as c_a.

The transmission characteristics of a curved section are plotted in Fig. 5. It is noticed from the figure that, at lower frequencies where the effect of the trough is more pronounced, the transmission characteristics of the image guide are improved except for the $c = 2$-mm case where it is believed that the scattering at the transition is quite strong. When we remove the inside wall, the loss decreases considerably as shown by $c_a = 2$-mm curve. Since $c_a = 4$-mm case is indistinguishable on the graph, only $c = 4$-mm case is shown. Notice that the transmission characteristics in Fig. 5 include the scattering loss at transitions from the image guide to the trapped image guide.

Since radiation also occurs at the transition from the image guide to the trapped image guide, we find that the radiation loss caused in the curved section itself should be smaller than those in Fig. 5. To confirm our argument, we have measured two other quantities. The first is the reflection toward the microwave source from the dielectric waveguide setup including the transitions. The results indicate that the reflection is generally quite small (less than -20 dB) and its characteristics do not depend on the different arrangement of the dielectric waveguide. This fact dictates that most of the energy scattered in the dielectric waveguide section is radiated and is not coupled to the metal waveguide mode through the transition.

The second quantity we measured is the radiated energy. Since the radiation occurs at several different locations, viz., at the transition to the image guide, at the image guide to trapped image guide transition and finally at the bend, it is desirable to distinguish these components. Although complete distinction is not possible, we tried to receive the energy radiated at the bend most strongly. To this end, we placed a standard gain horn at about 5 cm away from the outer wall of the image guide wall location. The axis of the horn is on the radius of curvature intersecting the midpoint of the curved section. Therefore, the horn is looking at the setup in a symmetric manner.

Fig. 6 shows the frequency characteristics of the radiated power captured by the horn. Only the results for $c = 4$-mm case and the image guide case ($c \to \infty$) are plotted to avoid crowded drawings as in the other cases, i.e., $c = 2$, $c_a = 2$, and $c_a = 4$ mm gave results similar to those for $c = 4$-mm case. At lower frequencies, we see considerable reduction in radiation by the presence of the trough walls. It is, however, not possible to quantitatively compare different trapped image guide setups with each other, because radiations from several different sources are intermixed and the relative contributions from these sources will not be identical in each case.

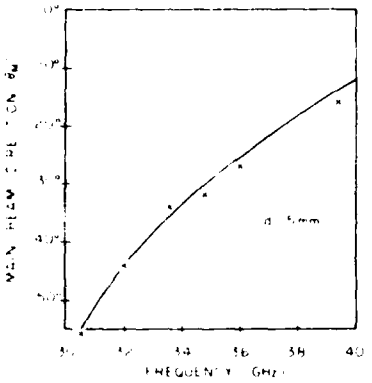

Fig. 7. Computed and measured (x) main beam direction.

IV. Grating Leaky-Wave Structures

The new waveguide is still an open waveguide as the trough is not covered. It is well known that, when periodic perturbations (gratings) are created in an open waveguide, the resulting structure exhibits either the leaky wave or surface wave passband and stopband phenomena [5], [6].

The structure works as a frequency-scannable antenna if $|\beta_n/k_0|<1$ where k_0 is the free space wavenumber and $\beta_n=\beta+2n\pi/d$ is the propagation constant of the nth space harmonic associated with the grating with the period d. The main beam direction measured from the broadside is given by

$$\theta_M=\sin^{-1}\left(\frac{\beta}{k_0}+\frac{n\lambda}{d}\right). \tag{6}$$

Usually, n is taken to be -1. It is seen from (6) that θ_M is a function of frequency. If the attenuation of the guided wave due to radiation is small in the grating the radiation pattern is approximated by that of the cophasally excited linear array, and may be obtained from the well-known space factor calculation. Then, the power radiation is given by

$$S(\theta)=\frac{1}{N^2}\left|\frac{\sin(N\psi/2)}{\sin(\psi/2)}\right|^2 \tag{7}$$

$$\psi=k_0 d\sin\theta-\beta_n d \tag{8}$$

where N is the number of grating elements.

We developed an antenna from the trapped image guide with $\epsilon_r=2.56$, $a=b=2$ mm, $h=4$ mm, $c=4$ mm. The grating period was taken as $d=5$ mm and the number of elements was 28. The grating was created with narrow (1 mm wide) metal strips placed on the top surface of the dielectric rod. Fig. 7 shows the computed and measured main beam directions when the frequency is changed in the *Ka* band. The negative values of θ_M imply that the antenna is backward firing. The differences in theory and experiments are mostly less than 2°. Fig. 8 shows a typical E-plane (yz-plane) radiation pattern. The pattern is a bit asymmetric as the antenna was placed near the edge of a big metallic slab. A relatively strong radiation in the $+72°$ is caused by the fact that the transmitting oscillator radiated power directly into the feed horn of the antenna. The main beam width and sidelobe levels computed by the simple theory above resulted 6° (at -3dB) and -13.5dB as compared with measured values of 6.5° and -14dB.

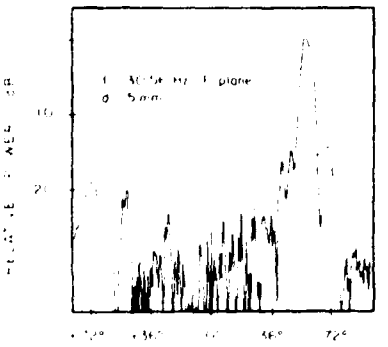

Fig. 8. Radiation pattern.

V. Conclusions

We proposed a novel trapped image guide for millimeter wave applications for the purpose of reducing the radiation loss at curved sections. Fundamental propagation characteristics are obtained by an approximate theory. Numerical results are compared with measured data. Investigations of radiation loss at a 90° curved section as well as the application of this guide to a leaky-wave radiator are included.

References

[1] R. M. Knox, "Dielectric waveguide microwave integrated circuits—An overview," *IEEE Trans. Microwave Theory Tech.*, vol. MTT-24, pp. 806–814, Nov. 1976.

[2] H. Jacobs, G. Novick, C. M. LoCascio, and M. M. Chrepta, "Measurement of guide wavelength in rectangular dielectric waveguides," *IEEE Trans. Microwave Theory Tech.*, vol. MTT-24, pp 815–820, Nov. 1976.

[3] W. McLevige, T. Itoh, and R. Mittra, "New waveguide structures for millimeter wave and optical integrated circuits," *IEEE Trans Microwave Theory Tech.*, vol. MTT-23, pp. 788–794, Oct. 1975.

[4] T. Itoh, "Inverted strip dielectric waveguide for millimeter-wave integrated circuits," *IEEE Trans. Microwave Theory Tech.*, vol. MTT-24, pp. 821–827, Nov. 1976.

[5] T. Itoh, "Applications of gratings in a dielectric waveguide for leaky-wave antennas and band-reject filters," *IEEE Trans. Microwave Theory Tech.*, vol. MTT-25, pp. 1134–1137, Dec. 1977.

[6] B. S. Song and T. Itoh, "Distributed Bragg reflection dielectric waveguide oscillators," *IEEE Trans. Microwave Theory Tech.*, vol. MTT-27, pp. 1019–1022, Dec. 1979.

APPENDIX 4

DIRECTIVE PLANAR EXCITATION OF AN IMAGE-GUIDE

Y. Shih, T. Rivera, and T. Itoh

Dept. of Electrical Engineering
The University of Texas
Austin, Texas 78712

ABSTRACT

An image guide is excited by a Slot Yagi-Uda array created in the ground plane so that the majority of the energy travels in a specified direction. The method is useful for implementing planar devices for image-guide structures.

Introduction

Recently, image-guides have been investigated by a number of workers for application in millimeter-wave integrated circuits.[1,2] To date, an image-guide is typically excited by a tapered section inserted into an open-ended waveguide or a waveguide horn designed for the least amount of insertion loss and reflection. These structures with good design are useful for interfacing the image-guide with conventional waveguide circuits. However, if true millimeter-wave integrated circuits are built with image-guide structures, it is necessary that solid state devices are incorporated in or near the image guide so that they interface the latter directly or possibly by way of planar networks such as microstrips. Direct implementation of solid state devices is not very rewarding as the junction created by the device causes a number of problems such as radiation and impedance mismatch.

To alleviate such problems, Solbach recently proposed a slot structure in the ground plane of the image-guide and placed a detector diode in the slot.[3] With an appropriate design, detector efficiency was found to be relatively good. One of the problems of such a structure, however, is that the slot created in the ground plane is bidirectional, that is, it captures the guided waves coming from both directions. Or if the slot is used for excitation, the power is split into both directions in the image-guide.

This paper proposes a method for substantially increasing the directivity of the excitation from the slot in the ground plane. This scheme consists of multi-slots in the ground plane arranged in a Yagi-Uda array arrangement (Figure 1). Unlike the phased array arrangement, the Yagi-Uda array requires only one element to be active, thus reducing the number of required active devices. Actually, a monopole type Yagi-Uda array inserted into the dielectric guide has been reported.[4] However, the present structure is much more appropriate for millimeter-wave circuits because the slot structures are amenable to planar fabrication technology.

Design Criteria

The slots in the ground plane of an image guide can behave as the elements of a Yagi-Uda array by adjusting the width, length, and spacing of the slots. The parameters of interest are defined in Figure 1.

This work was supported in part by U.S. Army Research Office Grant DAAG29-78-G-0145, and in part by Joint Services Electronics Program F49620-77-C-0101.

The length of the driving element is chosen so that it is at half-wavelength resonance. Note that the slot can be viewed as a short-circuited slot-line with the dielectric slab of the image-guide as the substrate. Hence, to determine the resonant length, the analysis developed by S. Cohn[5,6] was utilized and yielded a second-order approximation for the guided wavelength. Design data was available from various curves in Cohn's analysis and the slot-line parameters were substituted to give the length of the resonant slot. In addition, the end effect in a shorted slot had to be taken into account. Research conducted by Knorr and Saenz[7] indicates that this factor serves to increase the resonant length by as much as 20%.

To obtain the maximum excitation of the image-guide mode in one direction, it is necessary to adjust the Yagi-Uda slot parameters. By lengthening and shortening the parasitic slots, reflector and director elements are created to increase the coupled energy along a specified direction. The research conducted by several authors[8,9] indicates that the reflector length is approximately 5% longer than that of the driver and the director is about 10% shorter.

The optimum reflector spacing was experimentally determined[8] to be $\lambda_g/4$. As for the director spacing, a maximum gain can be achieved by adjusting the width and length of the slot as long as such spacing does not exceed $0.5\lambda_g$. Note that λ_g in our application should be the guide wavelength of the E^y_{11} mode in the image line, and is determined by applying the method of effective dielectric constants.[10] To this end, we first obtain ε_{eff} for the vertically polarized modes

$$\varepsilon_{eff} = \varepsilon_r - \left(\frac{k_y}{k_0}\right)^2 \qquad (1)$$

where k_y is the solution to the eigenvalue equation

$$\left(\frac{k_y}{\varepsilon_r}\right) \tan k_y b = \sqrt{(\varepsilon_r - 1) k_0^2 - k_y^2} \qquad (2)$$

Next, the structure is replaced with a hypothetical vertical slab of width $2a$ and infinite height and dielectric constant ε_{eff}. By solving the eigenvalue equation of this hypothetical structure for the phase constant, k_x, in the slab region, we obtain the propagation constant of the guide mode from $k_z = \sqrt{\varepsilon_{eff} k_0^2 - k_x^2}$, and thus, the guided wavelength, λ_g.

Finally, the width of the slots is adjusted to vary the input impedance so that the optimum gain is obtained. Rigorous determination of the impedance is too complex to be practical for this study, and thus the slot widths were determined experimentally.

Although an active device may be directly implemented in the driving slot, our objective here is to study the coupling between the slot array and the image-guide. To this end, we studied several methods of exciting the slot by an external source. Fig. 3a is one of such structures. Although this configuration deviates from the planar type design, a good impedance match can easily be obtained to enhance efficient excitation of the driving slot. It is thus appropriate for laboratory studies. Figure 3b proposes a planar type feed with a slot-line. Design of an efficient feed by this mechanism is more difficult.

Experimental Results

Various configurations were tested and the following parameters were used: a design frequency of 7.5 GHz, a ground plane thickness of 0.1 mm, and a dielectric constant of 10.0. Yagi arrays with only two elements (driver and reflector, driver and director) were tested first. The measured front-to-back ratios of transmitted power are shown in Figure 4. A relatively high ratio is obtained with the reflector behind the driving slot. However, the bandwidth is very narrow. A wider bandwidth (but a lower ratio) appears in the case of the driver and director when the width of the director is larger. By introducing more directors into the array, a higher ratio and wider bandwidth is obtained. The results for 3, 4, and 5 element arrays are shown in Figure 5.

Conclusion

The principles of the Yagi-Uda array are applied to the slot-fed image line in order to reduce the radiation losses and increase the energy transmitted in the specified direction. The experimental results show that even with a two-element design, one can obtain greater transmission in the forward direction. A five-element design proved to have a wider bandwidth while maintaining an overall increase in directivity in the desired direction. The results reported in this paper are believed to be viable and can prove to be effective in the design of planar millimeter-wave circuits using image-guide structures. It is expected that an increased number of director elements improve the front to back excitation ratio even further, provided a careful design is carried out.

References

1. B-S. Song, T. Itoh, "Distributed Bragg Reflection Dielectric Waveguide Oscillators," IEEE Trans. MTT, vol. MTT-27, No. 12, pp. 1019-1022, December 1979.

2. J. A. Paul and Y.-W. Chang, "Millimeter wave image-guide integrated passive devices," IEEE Trans. MTT, vol. MTT 26, No. 10, pp. 751-754, October 1978.

3. K. Solbach, "Slots in dielectric image line as mode launchers and circuit elements," IEEE Trans. MTT, accepted for publication, paper no. k-214.

4. W. K. McRitchie and J. C. Beal, "Yagi-Uda array as a surface-wave launcher for dielectric image lines," IEEE Trans. MTT, vol. MTT 20, pp. 193-196, August 1972.

5. S. B. Cohn, "Slot line on a dielectric substrate," IEEE Trans. MTT, vol. MTT 17, pp. 768-778, October 1969.

6. E. A. Mariana, et. al., "Slot line characteristics," IEEE Trans. MTT, vol. MTT 17, pp. 1091-1096, December 1969.

7. J. B. Knorr and J. Saenz, "End effect in a shorted slot," IEEE Trans. MTT, vol. 21, pp. 579-580, September 1973.

8. H. W. Ehrenspeck and H. Poehler, "A new method for obtaining maximum gain from Yagi antennas," IRE Trans. on Antennas and Propagation, vol. Ap-7, pp. 379-386, October 1959.

9. K. M. Fishenden and E. R. Wiblin, "Design of Yagi aerials," Proc. IEE (London), vol. 96, pt. III, pp. 5-12, March 1959.

10. T. Itoh and B. Adelseck, "Trapped image guide for millimeter-wave circuits," IEEE Trans. MTT, vol. MTT-28, pp. 1433-1436, December 1980.

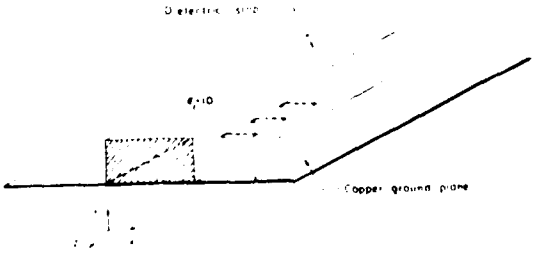

FIGURE 1 SLOT-FED DIELECTRIC IMAGE LINE.

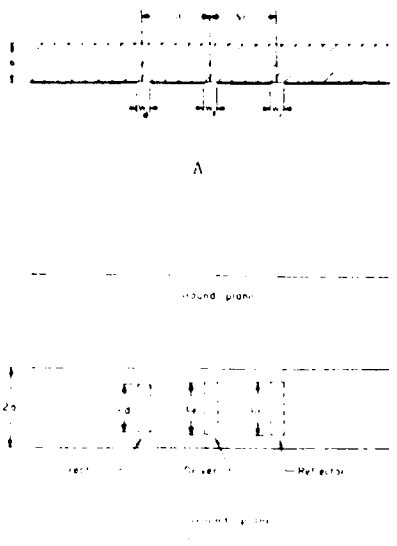

FIGURE 2: DIMENSIONS OF DIELECTRIC IMAGE LINE, (A) SIDE VIEW, (B) TOP VIEW.

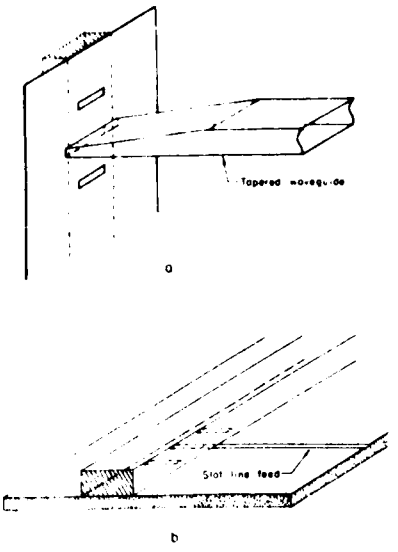

FIGURE 3: FEEDING METHODS, (A) REDUCED HEIGHT WAVEGUIDE FEED, (B) SLOT LINE FEED.

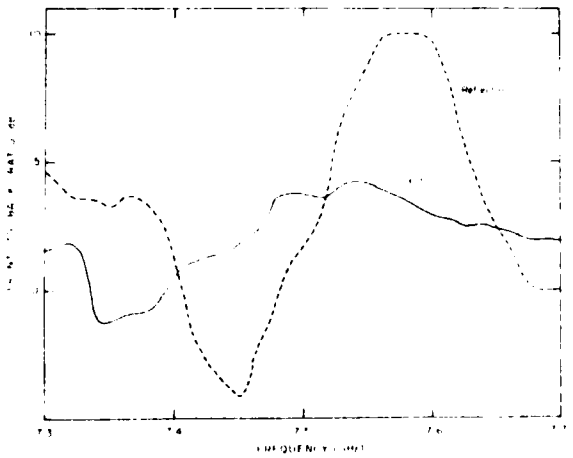

FIGURE 4: FRONT-TO-BACK POWER RATIO VS. FREQUENCY (REFLECTOR CASE: L_f = 7.8 mm, W_f = 0.5 mm, L_r = 8.2 mm, W_r = 0.3 mm, S_r = 3.5 mm; DIRECTOR CASE: L_f = 7.9 mm, W_f = 1.0 mm, L_d = 7.2 mm, W_d = 1.0 mm, S_d = 3.4 mm).

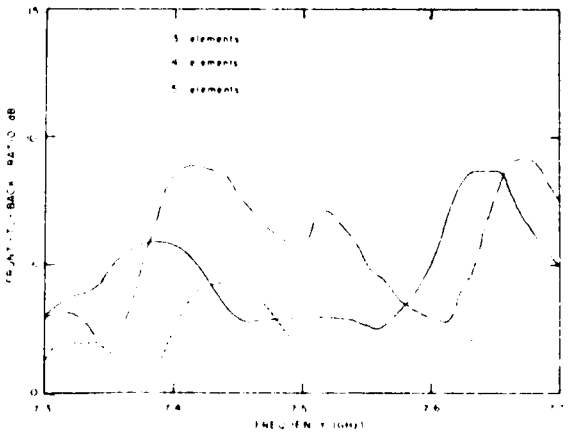

FIGURE 5: FRONT-TO-BACK POWER RATIO VS. FREQUENCY FOR MULTI-ELEMENT ARRAYS (L_f = 7.8 mm, W_f = 0.5 mm, L_r = 8.2 mm, W_r = 0.3 mm, S_r = 3.5 mm, L_d = 7.0 mm, W_d = 0.6 mm, S_d = 5.2 mm).

APPENDIX 5

MILLIMETER-WAVE PLANAR SLOT ANTENNAS WITH DIELECTRIC FEEDS

P. Yen and L. A. Paul
Hughes Aircraft Company
Electron Dynamics Division
3100 West Lomita Boulevard
Torrance, CA 90509

T. Itoh
Dept. of Electrical Engineering
University of Texas
Austin, Texas 78712

ABSTRACT

Measurements have been made on various antenna configurations suitable for monolithic integration at millimeter-wave frequencies. The basic structure consists of a single slot dipole radiator etched on a dielectric substrate and combined with a beam lead detector diode. Enhancement of the antenna directivity has been achieved through the use of dielectric rods oriented over the slot area. Addition of these rods has improved directivity up to 10 dB at 60 GHz.

Introduction

There is an ever increasing interest in the application of monolithic fabrication techniques to millimeter-wave components.[1-3] One such objective of monolithic integration is to eliminate the use of waveguide connections to a circuit, including those from an antenna to a mixer. In order to do so, an efficient antenna structure must be developed which can be combined with quasi-optical or other such techniques to fulfill the overall directivity requirements of the system.

One antenna structure being investigated is the planar slot dipole. By combining a dipole etched on a dielectric substrate with a dielectric rod feed oriented over the slot area, the directivity is improved and field pattern is suitable for feeding a parabolic or Cassegrain structure.

Slot Antenna

The slot antenna is an adaptation of a rather classical design[4,5] that uses two shorted quarter-wavelength transmission lines. In this specific case, a coplanar waveguide transmission line is used to feed a half-wave slot dipole at the center. Figure 1 shows the layout of the antenna and feed. A bonding pad is included at the end of the feed for bonding a beam lead diode and video output line. This pad can also serve for bonding a detector bypass capacitance to the surrounding ground plane.

Various dielectric substrate materials have been used for the slot antenna including Duroid, Teflon, quartz, Al_2O_3, sapphire, and high resistivity silicon. The two materials most thoroughly evaluated to date are Teflon and quartz. For the 60 GHz antenna design, the Teflon substrates were 30 mil thick with 15 μm of copper cladding, while the quartz substrates were 250 mil thick with plated up Cr-Au metallization.

Initial tests showed the detector output voltage to be lower than expected due to insufficient bypass capacitance for the diode. Additional capacitance was added by strapping two thin film capacitors to the bonding pad as shown in Figure 2. This additional capacitance increased the detected output voltage by 20 dB, thus improving the overall efficiency.

Dielectric Feed

The directivity of a simple slot dipole[2] is rather poor if being considered as a feed for an antenna system. To enhance the directivity, a rectangular dielectric rod was placed over the dipole area. It is well known that the dielectric rod can be used as a surface wave antenna.[6] In the present work, such a surface wave antenna rod is used as a director to enhance the directivity of the slot antenna. Tapering of the rod in one or both dimensions improved the VSWR and prevented severe aberrations in the radiation pattern. Dielectric materials for the rods were chosen to be compatible with the slot antenna substrate. For the Teflon substrate, rods were made of Teflon. However, to simplify fabrication of the rods for the quartz substrate structures, boron nitride was used for the rods rather than quartz.

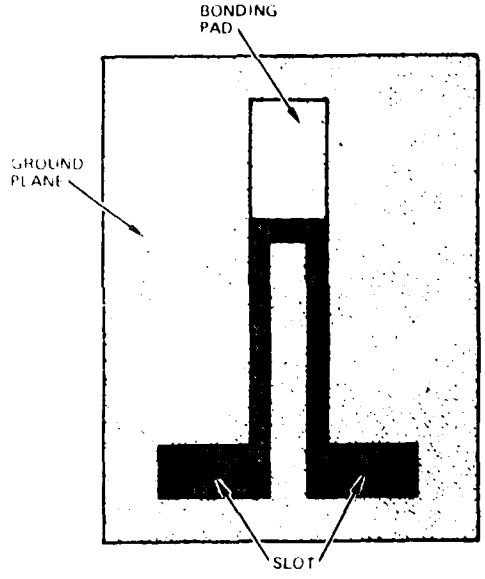

FIGURE 1 60 GHz SLOT DIPOLE ANTENNA

Design of the dielectric rods was based upon single mode propagation of dielectric waveguide. The overall length of the rod was typically 3 to 5 free space wavelengths with a tapered section about half the overall length. Figure 3 shows a typical dielectric rod. Although the overall antenna performance may be improved further by more extensive design procedure of the rod structure, the present attempt exhibited more than satisfactory results, as shown later.

Rods were attached to the slot antenna by means of a polystyrene based adhesive. Its low dielectric constant and low loss nature assured little perturbation in the radiation pattern due to its presence.

FIGURE 2 BYPASS CAPACITOR [illegible]

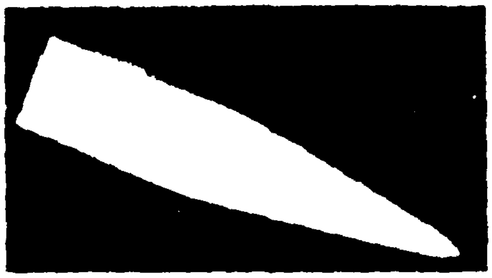

[illegible] PLANE VIEW

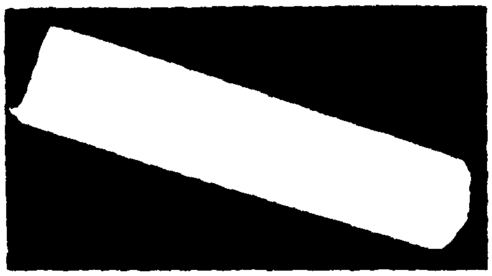

[illegible] PLANE VIEW

[illegible] DIELECTRIC [illegible]

[illegible] Test Setup

Field patter[illegible] anechoic chamber [illegible] A 59.75-GHz IMPATT [illegible] 1 kHz and radiate[illegible] antenna/detector [illegible] tally controlled rotat[illegible] transmitter. A bias supply [illegible] output voltage [illegible] signal before the [illegible] The rotation platform [illegible] to be made. [illegible] reorienting the [illegible]

[illegible] that are now be [illegible] rotation where some con[illegible] structure.

[illegible]

For a give[illegible] made on the [illegible] in order to [illegible] dielectric rod [illegible] side, and then [illegible] patterns were [illegible] and 15 show the patterns for [illegible] designs. All of the patterns have been [illegible] the patterns with the [illegible] a rod significantly [illegible] increases the [illegible] addition, it is possible to [illegible] beam into either the [illegible] or the substrate [illegible]

[illegible] a feature [illegible] which exhibits high [illegible] indicate that this [illegible] applic[illegible]

[illegible] application to [illegible] Patterson, Ohio, [illegible] Dershan as [illegible] order of it

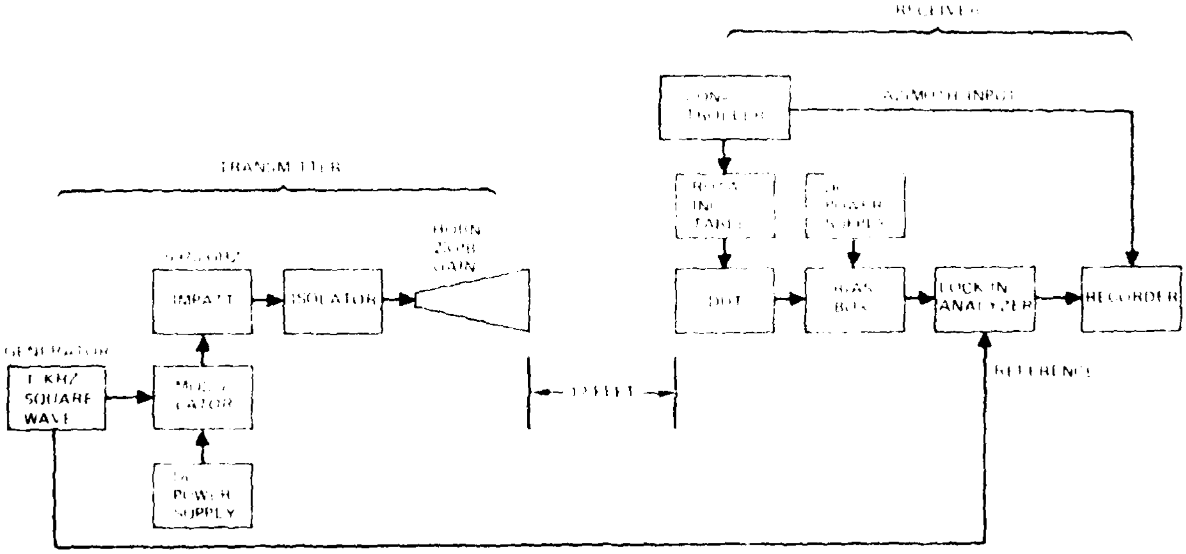

FIGURE 4 PATTERN MEASUREMENT TEST SETUP

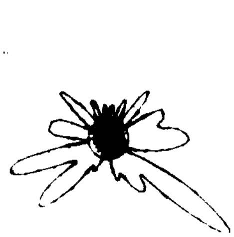

FIGURE 5(a) TEFLON SLOT [illegible]
ANTENNA E-PLANE

FIGURE 5[illegible] [illegible]
ANTENNA [illegible]

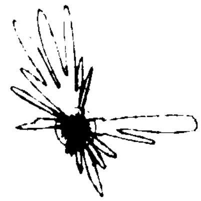

[illegible] QUARTZ SLOT
ANTENNA [illegible]

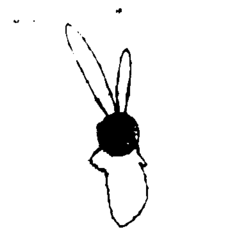

FIGURE 5[illegible] QUARTZ SLOT
ANTENNA H-PLANE

FIGURE [illegible] ANTENNA
WITH ROD E-PLANE

[illegible] ANTENNA
WITH ROD [illegible]

[illegible] ANTENNA
[illegible]

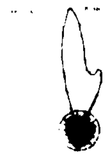

FIGURE 6[illegible] QUARTZ ANTENNA
WITH BN ROD H-PLANE

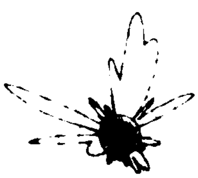

FIGURE [illegible] ANTENNA
WITH [illegible] E-PLANE

[illegible]
[illegible]

[illegible] ANTENNA
[illegible]

FIGURE 8(b) QUARTZ ANTENNA
WITH BN ROD H-PLANE

number DAA[illegible] for the [illegible]. The authors also [illegible] Betty Mac[illegible] for their technical assistance and Dr. [illegible] diodes.

References

1. D.B. [illegible], S.[illegible], [illegible], D.[illegible] Angelakos, [illegible] "[illegible] and Waveguides [illegible] Integrated [illegible]," IEEE Journal [illegible], Vol. [illegible], No. [illegible], pp. 578-5[illegible], Ma[illegible].

2. [illegible]R. Kerr, [illegible] and [illegible] Matt[illegible], "A Simple [illegible] GHz," [illegible] IEEE MTT-S International Microwave Symposium Digest, IEEE Cat. No. [illegible] MTT, pp. 96-98, [illegible].

3. [illegible] "Schottky Diode Receivers for Operation in the [illegible] GHz Region," IERE, The Radio and Electronic Engineer, Vol. 49, No. 7/8, pp. 333-346, July/August 1979.

4. [illegible] Jasik, Antenna Engineering Handbook, New York, McGraw Hill Book Company, 1961.

5. J. D. Kraus, Antenna, New York, McGraw Hill Book Company, 1961.

6. Y. Shiau, "Dielectric Rod Antennas for Millimeter-wave Integrated Circuits," IEEE Transactions on Microwave Theory and Techniques, Vol. MTT-24, pp. 869-872, November 1976.

Spectral Domain Immitance Approach for Dispersion Characteristics of Generalized Printed Transmission Lines

TATSUO ITOH, SENIOR MEMBER, IEEE

Abstract—A simple method for formulating the dyadic Green's functions in the spectral domain is presented for generalized printed transmission lines which contain several dielectric layers and conductors appearing at several dielectric interfaces. The method is based on the transverse equivalent transmission line for a spectral wave and on a simple coordinate transformation. This formulation process is so simple that often it is accomplished almost by inspection of the physical cross-sectional structure of the transmission line. The method is applied to a new versatile transmission line, a microstrip-slot line, and some numerical results are presented.

I. Introduction

A FEW YEARS AGO, a method called the spectral-domain technique was developed for efficient numerical analyses for various planar transmission lines and successfully applied to a number of structures [1], [2]. One difficulty in applying this technique is that a lengthy derivation process is required in the formulation stage, especially for the more complicated structures such as the one recently proposed by Aikawa [3], [4] in which more than one conductor are located at different dielectric interfaces. This paper presents a simple method for deriving the dyadic Green's functions (immittance functions) which is based on the transverse equivalent circuit concept as applied in the spectral domain in conjunction with a simple coordinate transformation rule. This technique is quite versatile and the formulation of the Green's function may be done almost by inspection in many structures. It is noted that symmetry in the structure is not required and that the analysis can be extended to finite circuit elements, such as the disk resonator.

In what follows, we first illustrate the formulation process for the microstrip line and subsequently extend it to a more general microstrip-slot structure. Numerical results for the microstrip-slot structure are also presented.

II. Illustration of the Formulation Process

To illustrate the formulation process, we will use a simple shielded microstrip line shown in Fig. 1. In conventional space-domain analysis [5], this structure may be analyzed by first formulating the following coupled homogeneous integral equations and then solving for the unknown propagation constant β:

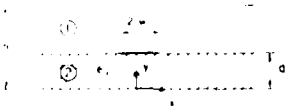

Fig. 1. Cross section of a microstrip line.

$$\int \left[Z_{zz}(x-x',d)J_z(x') + Z_{zx}(x-x',d)J_x(x') \right] dx' = 0 \tag{1}$$

$$\int \left[Z_{xz}(x-x',d)J_z(x') + Z_{xx}(x-x',d)J_x(x') \right] dx = 0 \tag{2}$$

where J_x and J_z are unknown current components on the strip and the Green's functions (impedance functions) Z_{zz}, etc., are functions of unknown β as well. The integration is over the strip, and (1) and (2) are valid on the strip. The left-hand sides of these equations give E_z and E_x components on the strip and, hence, are required to be zero to satisfy the boundary condition at the perfectly conducting strip. These equations may be solved provided that Z_{zz}, etc., are given. However, for the inhomogeneous structures, these quantities are not available in closed forms.

In the spectral domain formulation, we use Fourier transforms of (1) and (2) and deal with algebraic equations

$$\tilde{Z}_{zz}(\alpha,d)\tilde{J}_z(\alpha,d) + Z_{zx}(\alpha,d)\tilde{J}_x(\alpha,d) = \tilde{E}_z(\alpha,d) \tag{3}$$

$$\tilde{Z}_{xz}(\alpha,d)\tilde{J}_z(\alpha,d) + Z_{xx}(\alpha,d)\tilde{J}_x(\alpha,d) = \tilde{E}_x(\alpha,d) \tag{4}$$

instead of the convolution-type coupled integral equations (1) and (2). In (3) and (4), quantities with $\sim$ are Fourier transforms of corresponding quantities without $\sim$. The Fourier transform is defined as

$$\phi(\alpha) = \int_{-\infty}^{\infty} \phi(x) e^{j\alpha x} dx. \tag{5}$$

Notice that the right-hand sides of (3) and (4) are no longer zero because they are the Fourier transforms of E_z and E_x on the substrate surface which are obviously nonzero except on the strip. Hence, algebraic equations (3) and (4) contain four unknowns $\tilde{J}_z$, $\tilde{J}_x$, $\tilde{E}_z$, and $\tilde{E}_x$. However, $\tilde{E}_z$ and $\tilde{E}_x$ will be eliminated later in the solution process based on the Galerkin's procedure.

Manuscript received October 26, 1979, revised February 2, 1980. This work was supported in part by U.S. Army Research Office under Grant DAAG29-78-G-0145.

The author is with the Department of Electrical Engineering, University of Texas, Austin, TX 78712.

0018-9480/80/0700-0733$00.75 © 1980 IEEE

APPENDIX 6

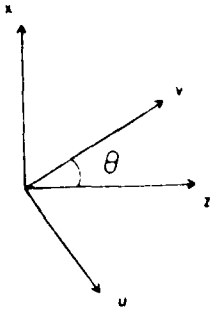

Fig. 2. Coordinate transformation

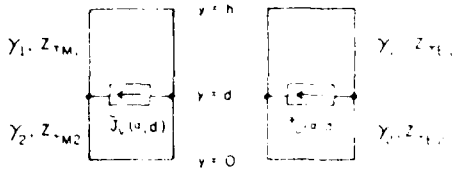

Fig. 3. Equivalent transmission lines for the microstrip line.

The closed forms of Green's impedance functions $\tilde{Z}_{zz}$, etc., can be derived by first writing the Fourier transforms of field components in each region in terms of superposition of TM-to-y and TE-to-y expressions by way of Maxwell's equations.

$$\tilde{E}_y(\alpha,y) = A^e \cosh \gamma_1 y, \qquad 0<y<d$$
$$= B^e \cosh \gamma_2 (h-y), \qquad d<y<h \tag{6}$$
$$\tilde{H}_y(\alpha,y) = A^h \sinh \gamma_1 y, \qquad 0<y<d$$
$$= B^h \sinh \gamma_2 (h-y), \qquad d<y<h \tag{7}$$
$$\gamma_1 = \sqrt{\alpha^2+\beta^2-\epsilon_r k^2} \qquad \gamma_2 = \sqrt{\alpha^2+\beta^2-k^2}. \tag{8}$$

Next, we match tangential (x and z) components at the interface and apply appropriate boundary conditions at the strip [1], [2]. By eliminating A^e, B^e, A^h, and B^h from these conditions, we obtain expressions for Green's impedance functions $\tilde{Z}_{zz}$, etc.

In the new formulation process we will make use of equivalent transmission lines in the y direction. To this end, we recognize that from

$$E_y(x,y)e^{-j\beta z} = \frac{1}{2\pi}\int_{-\infty}^{\infty} E_y(\alpha,y)e^{-j(\alpha x+\beta z)}d\alpha \tag{9}$$

all the field components are a superposition of inhomogeneous (in y) waves propagating in the direction of θ from the z axis where $\theta = \cos^{-1}(\beta/\xi)$, $\xi = \sqrt{\alpha^2+\beta^2}$. For each θ, waves may be decomposed into TM-to-y ($\tilde{E}_y, \tilde{E}_t, \tilde{H}_u$), and TE-to-$y$ ($\tilde{H}_y, \tilde{E}_u, \tilde{H}_t$) where the coordinates t and u are as shown in Fig. 2 and related with (x,z) via

$$u = z\sin\theta - x\cos\theta$$
$$t = z\cos\theta + x\sin\theta. \tag{10}$$

We recognize that $\tilde{J}_t$ current creates only the TM fields and $\tilde{J}_u$ the TE fields. Hence, we can draw equivalent circuits for the TM and TE fields as in Fig. 3. The characteristic admittances in each region are

$$Y_{TM_i} = \frac{\tilde{H}_u}{\tilde{E}_t} = \frac{j\omega\epsilon_0\epsilon_i}{\gamma_i}, \qquad i=1,2 \tag{11}$$
$$Y_{TE_i} = \frac{\tilde{H}_t}{\tilde{E}_u} = \frac{\gamma_i}{j\omega\mu}, \qquad i=1,2 \tag{12}$$

where $\gamma_i = \sqrt{\alpha^2+\beta^2-\epsilon_i k^2}$ is the propagation constant in the y direction in the ith region. All the boundary conditions for the TE and TM waves are incorporated in the equivalent circuits. For instance, the ground planes at $y=0$ and h are represented by short circuits at respective places. The electric fields $\tilde{E}_t$ and $\tilde{E}_u$ are continuous at $y=d$ and are related to the currents via

$$\tilde{E}_t(\alpha,d) = \tilde{Z}^e(\alpha,d)\tilde{J}_t(\alpha,d) \tag{13}$$
$$\tilde{E}_u(\alpha,d) = \tilde{Z}^h(\alpha,d)\tilde{J}_u(\alpha,d). \tag{14}$$

$\tilde{Z}^e$ and $\tilde{Z}^h$ are the input impedances looking into the equivalent circuits at $y=d$ and are given by

$$\tilde{Z}^e(\alpha,d) = \frac{1}{Y_1^e + Y_2^e} \tag{15}$$
$$\tilde{Z}^h(\alpha,d) = \frac{1}{Y_1^h + Y_2^h} \tag{16}$$

where Y_1^e and Y_2^e are input admittances looking down and up at $y=d$ in the TM equivalent circuit and Y_1^h and Y_2^h are those in the TE circuit:

$$Y_1^e = Y_{TM_1}\coth\gamma_1(h-d) \qquad Y_2^e = Y_{TM_2}\coth\gamma_2 d \tag{17}$$
$$Y_1^h = Y_{TE_1}\coth\gamma_1(h-d) \qquad Y_2^h = Y_{TE_2}\coth\gamma_2 d \tag{18}$$

The final step consists of the mapping from the (u,t) to (x,z) a coordinate system for the spectral wave corresponding to each θ given by α and β. Because of the coordinate transform (10), E_x and E_z are linear combinations of E_u and E_t. Similarly, J_x and J_z are superpositions of J_u and J_t. When these relations are used, the impedance matrix elements in (3) and (4) are found to be

$$\tilde{Z}_{zz}(\alpha,d) = N_z^2\tilde{Z}^e(\alpha,d) + N_x^2\tilde{Z}^h(\alpha,d) \tag{19}$$
$$\tilde{Z}_{zx}(\alpha,h) = \tilde{Z}_{xz}(\alpha,d) = N_x N_z\left[-\tilde{Z}^e(\alpha,d) + \tilde{Z}^h(\alpha,d)\right] \tag{20}$$
$$\tilde{Z}_{xx}(\alpha,d) = N_x^2\tilde{Z}^e(\alpha,d) + N_z^2\tilde{Z}^h(\alpha,d) \tag{21}$$

where

$$N_x = \frac{\alpha}{\sqrt{\alpha^2+\beta^2}} = \sin\theta \qquad N_z = \frac{\beta}{\sqrt{\alpha^2+\beta^2}} = \cos\theta. \tag{22}$$

Notice that $\tilde{Z}^e$ and $\tilde{Z}^h$ are functions of $\alpha^2+\beta^2$ and the ratio of α to β enters only through N_x and N_z.

It is easily shown that (19)–(21) are identical to those previously derived by means of boundary value problems imposed on the field expression [1], [2].

III. Extension to the Microstrip-Slot Structure

The method presented in the previous section may be extended to more complicated structures such as the microstrip-slot line structure in Fig. 4. This structure is

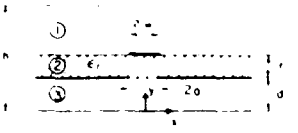

Fig. 4. Cross section of a microstrip-slot line.

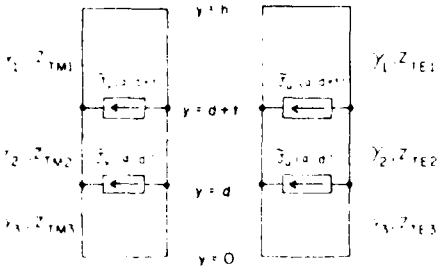

Fig. 5. Equivalent transmission lines for the microstrip-slot line.

believed to be useful in many microwave integrated circuit designs because there is an additional degree of freedom in design due to the existence of the slot [3], [4], [6]. The characteristic impedance and the propagation constant may be altered from those in the microstrip line by changing the slot width in the new structure.

By comparing the new structure with the microstrip line in Fig. 1, we may draw equivalent circuits in Fig. 5. From Fig. 5, we get

$$\tilde{E}_t(\alpha, d+t) = \tilde{Z}_{11}^t \tilde{J}_t(\alpha, d+t) + \tilde{Z}_{12}^t \tilde{J}_u(\alpha, d) \quad (23a)$$

$$\tilde{E}_u(\alpha, d+t) = \tilde{Z}_{11}^h \tilde{J}_u(\alpha, d+t) + \tilde{Z}_{12}^h \tilde{J}_u(\alpha, d) \quad (23b)$$

$$\tilde{E}_t(\alpha, d) = \tilde{Z}_{21}^t \tilde{J}_t(\alpha, d+t) + \tilde{Z}_{22}^t J_u(\alpha, d) \quad (24a)$$

$$\tilde{E}_u(\alpha, d) = \tilde{Z}_{21}^h \tilde{J}_u(\alpha, d+t) + \tilde{Z}_{22} \tilde{J}_u(\alpha, d) \quad (24b)$$

where $\tilde{Z}_{11}^t$ is the driving point input impedance at $y = d+t$ and $\tilde{Z}_{12}$ is the transfer impedance which expresses the contribution of the source at $y = d$ to the field at $y = d+t$. Other quantities may be similarly defined. Specifically

$$Z_{11}^t = \frac{1}{Y_1^t + Y_{2t}^t} \quad (25)$$

$$Y_1^t = Y_{TM1} \coth \gamma_1 (h - d - t) \quad (26)$$

$$Y_{2t}^t = Y_{TM2} \frac{Y_{TM2} + Y_3^t \coth \gamma_2 t}{Y_3^t + Y_{TM2} \coth \gamma_2 t} \quad (27)$$

where

$$Y_3^t = Y_{TM3} \coth \gamma_3 d. \quad (28)$$

It is readily seen that Y_3^t and Y_{2t}^t are input impedances looking down at $y = d$ and $d+t$, respectively, while Y_1^t is the one looking upward at $y = d+t$. On the other hand

$$\tilde{Z}_{12}^t = \frac{1}{Y_1^t + Y_{2u}^t} \frac{Y_{TM2}/\sinh \gamma_2 t}{Y_3^t + Y_{TM2} \coth \gamma_2 t} \quad (29)$$

Here

$$Y_{2u}^t = Y_{TM2} \frac{Y_{TM2} + Y_3^t \coth \gamma_2 t}{Y_3^t + Y_{TM2} \coth \gamma_2 t}$$

is the input admittance looking upward at $y = d$. We recognize that Z_{12}^t is the transfer impedance from Port 2 to Port 1 in the TM equivalent circuit. All other impedance coefficients in (23) and (24) may be similarly derived.

Impedance-matrix elements may be derived by the coordinate transform identical to the one used in the microstrip case. Some of the results are

$$\tilde{Z}_{zz}^{11} = N_z^2 \tilde{Z}_{11}^t + N_x^2 \tilde{Z}_{11}^h \quad (30)$$

$$\tilde{Z}_{zx}^{11} = N_z N_x (-\tilde{Z}_{11}^t + \tilde{Z}_{11}^h) \quad (31)$$

$$\tilde{Z}_{zz}^{12} = N_z^2 \tilde{Z}_{12}^t + N_x^2 \tilde{Z}_{12}^h. \quad (32)$$

The subscripts, say zx, indicate the direction of the field (E_z) caused by that of the contributing current (J_x). The superscripts, say 12, signify the relation between the interface where the field is observed (1) and the one where the current is present (2).

IV. Some Features of the Method

The method presented here is useful in solving many printed line problems. We will summarize the procedure for the formulation. 1) When the structure is given, we first draw TM and TE equivalent circuits. Each layer of dielectric medium is represented by different transmission lines and whenever conductors are present at particular interfaces, we place current sources at the junctions between transmission lines. At the ground planes, these transmission lines are shorted. 2) We derive driving point and transfer impedances from the equivalent circuits. 3) They are subsequently combined according to the sub- and superscript conventions described in the previous section, and we obtain the necessary impedance matrix elements.

The method has certain attractive features:

1) When the structures are modified, such changes are easily accommodated. For instance, when our structure has sidewalls, at say $x = \pm L$, to completely enclose the printed lines, all the procedures remain unchanged provided the discrete Fourier transform is used

$$\tilde{\phi}(\alpha) = \int_{-L}^{L} \phi(x) e^{j\alpha x} dx, \qquad \alpha = \frac{n\pi}{2L}. \quad (33)$$

On the other hand, when the top wall is removed, we only replace the shorted transmission line for the top-most layer with a semi-infinitely long one extending to $y \to +\infty$.

2) The formulation is independent of the number of strips and their relative location at each interface. Information on these parameters is used in the Galerkin's procedure to solve equations such as (3) and (4).

3) For some structures such as fin lines [8], it is more advantageous to use admittance matrix which provides the current on the fins due to the slot field. The formulation in this case almost parallels the present one. Instead of the current sources, we need to use voltage sources in the equivalent circuits.

4) It is easily shown that the method is applicable to finite structures such as microstrip resonators and antennas. Instead of (5), we need to use double Fourier transforms in x and z directions so that only the y dependence remains to allow the use of equivalent circuit concept.

5) Certain physical information is readily extracted. For instance, it is clear that denominators of typical impedance matrix elements give the transverse resonance equation when equated to zero. This implies that for certain spectral waves determined by α and β, surface wave poles may be encountered. How strongly the surface wave is excited, or if it is excited at all, is determined by the structure.

V. Numerical Example

Although the intention of this paper is to show the formulation process, the additional steps required to obtain numerical results are discussed for the sake of completeness. We computed dispersion characteristics of the microstrip-slot line with sidewalls at $x = \pm L$ by the present formulation followed by a Galerkin's procedure repeatedly used in the spectral-domain method.

In the previous section, the problem is formulated by using the impedance matrix with elements Z_{pq}^{ij}, $(i,j = 1,2$ and $p,q = x,z)$ and we presumed that the current components on the conductors are unknown. It is more advantageous in numerical calculation if we choose the current components on the strip $\tilde{J}_z(\alpha, d+t)$ and $\tilde{J}_x(\alpha, d+t)$ and the aperture fields in the slot $\tilde{E}_z(\alpha, d)$ and $\tilde{E}_x(\alpha, d)$ for unknowns in the Galerkin's procedure. This is because the aperture field in the slot can be more accurately approximated than the current on the conductor at $y = d$ [4], [7]. To this end, we rearrange the impedance matrix equation to the one in which the above four unknown quantities are on the left-hand side. This modification can be readily accomplished. In the Galerkin's method, these unknowns are expressed in terms of known basis functions. Finally, we obtain homogeneous linear simultaneous equations as the right-hand side becomes identically zero by the inner product process [1], [2]. By equating the determinant to zero, we find the eigenvalue β.

There are two types of modes in the structure. One of them is a perturbed microstrip mode and another is a perturbed slot mode. For the perturbed microstrip quasi-TEM mode, we have computed dispersion relations by choosing only one basis function each for four unknowns. They are chosen such that appropriate edge conditions are satisfied at the edges of strip and slot. For instance, we can choose as the basis functions the Fourier transforms of

$$J_z(x, d+t) = \frac{1}{\sqrt{w^2 - x^2}} \qquad J_x(x, d+t) = x\sqrt{w^2 - x^2}$$

$$E_z(x, d) = \sqrt{a^2 - x^2} \qquad E_x(x, d) = \frac{x}{\sqrt{a^2 - x^2}}$$

It is readily seen that Fourier transforms of these functions are analytically given in terms of Bessel functions. Fig. 6 shows some numerical examples of dispersion characteristics. The present results for a small slot width are compared with those of a shielded microstrip line [1]. It is clear that as the frequency increases, the presence of nonzero slot width becomes more significant. It is also seen that, as the slot width increases, the guide wavelength becomes larger because the effect for the free space below the slot is more pronounced. This suggests that the guide wavelength is adjustable by two means, one by changing the strip width and another by varying the slot width.

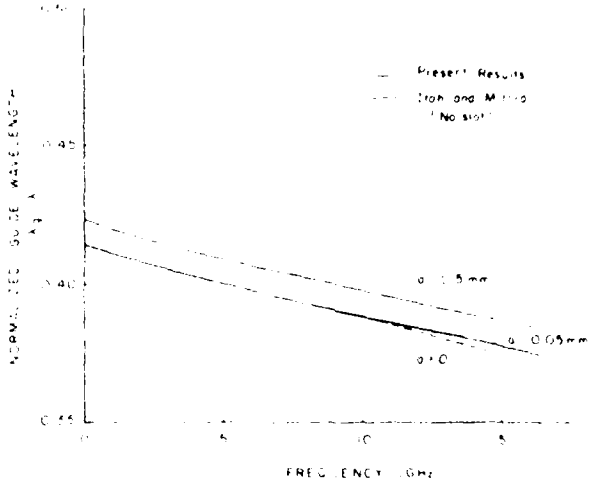

Fig. 6. Dispersion characteristics of microstrip-slot lines $L = 6.35$ mm, $d = 11.43$ mm, $t = 1.27$ mm, $h = 24.13$ mm, $w = 0.635$ mm, $\epsilon_r = 8.875$.

VI. Conclusions

We presented a simple method for formulating the eigenvalue problems for dispersion characteristics of general printed transmission lines. The method is intended to save considerable analytical labor for these types of problems. In addition, the method provides certain unique features. The method is applied to the problem of microstrip-slot line believed useful in microwave- and millimeter-wave integrated circuits. Numerical results are also presented.

References

[1] T. Itoh and R. Mittra, "A technique for computing dispersion characteristics of shielded microstrip lines," *IEEE Trans. Microwave Theory Tech.*, vol. MTT-22, pp. 896–898, Oct. 1974.

[2] T. Itoh, "Analysis of microstrip resonators," *IEEE Trans. Microwave Theory Tech.*, vol. MTT-22, pp. 946–952, Nov. 1974.

[3] M. Aikawa, "Microstrip line directional coupler with tight coupling and high directivity," *Electron. Commun. Jap.*, vol. J60-B, pp. 253–259, Apr. 1977.

[4] H. Ogawa and M. Aikawa, "Analysis of coupled microstrip-slot lines," *Electron. Commun. Jap.*, vol. J62-B, pp. 396–403, Apr. 1979.

[5] G. I. Zysman and D. Varon, "Wave propagation in microstrip transmission lines," presented at the Int. Microwave Symp. (Dallas, TX), May 1969, paper MAM-I-1.

[6] T. Itoh and A. S. Hebert, "A generalized spectral domain analysis for coupled suspended microstrip lines with tuning septums," *IEEE Trans. Microwave Theory Tech.*, vol. MTT-26, pp. 820–826, Oct. 1978.

[7] J. B. Davies and D. Mirshekar-Syahkal, "Spectral domain solution of arbitrary coupled transmission lines with multilayer substrate," *IEEE Trans. Microwave Theory Tech.*, vol. MTT-25, pp. 143–146, Feb. 1977.

[8] P. J. Meier, "Two new integrated circuit media with special advantages of millimeter wavelengths," presented at the 1972 IEEE G-MTT Int. Microwave Symp. (Arlington Heights, IL), May 1972.

END

DATE
FILMED

5-81

DTIC